

Alma Mater Studiorum Università di Bologna
Archivio istituzionale della ricerca

Anticancer and antibacterial potential of robust Ruthenium(II) arene complexes regulated by choice of α -diimine and halide ligands

This is the final peer-reviewed author's accepted manuscript (postprint) of the following publication:

Published Version:

Zanda E., Busto N., Biancalana L., Zacchini S., Biver T., Garcia B., et al. (2021). Anticancer and antibacterial potential of robust Ruthenium(II) arene complexes regulated by choice of α -diimine and halide ligands. CHEMICO-BIOLOGICAL INTERACTIONS, 344, 1-13 [10.1016/j.cbi.2021.109522].

Availability:

This version is available at: <https://hdl.handle.net/11585/848332> since: 2023-06-09

Published:

DOI: <http://doi.org/10.1016/j.cbi.2021.109522>

Terms of use:

Some rights reserved. The terms and conditions for the reuse of this version of the manuscript are specified in the publishing policy. For all terms of use and more information see the publisher's website.

This item was downloaded from IRIS Università di Bologna (<https://cris.unibo.it/>).
When citing, please refer to the published version.

(Article begins on next page)

This is the final peer-reviewed accepted manuscript of:

E. Zanda, N. Busto, L. Biancalana, S. Zacchini, T. Biver, B. Garcia, F. Marchetti, "Anticancer and antibacterial potential of robust Ruthenium(II) arene complexes regulated by choice of α -diimine and halide ligands", *Chem. Biol. Inter.*, **2021**, 344, 109522.

The final published version is available online at:

<https://doi.org/10.1016/j.cbi.2021.109522>

Terms of use:

Some rights reserved. The terms and conditions for the reuse of this version of the manuscript are specified in the publishing policy. For all terms of use and more information see the publisher's website.

Anticancer and Antibacterial Potential of Robust Ruthenium(II) Arene Complexes Regulated by Choice of α -Diimine and Halide Ligands

Emanuele Zanda,^a Natalia Busto,^{b,} Lorenzo Biancalana,^{a,*} Stefano Zacchini,^c Tarita Biver,^d Begoña
Garcia,^b Fabio Marchetti^{a,*}*

^a *Dipartimento di Chimica e Chimica Industriale, Università di Pisa, Via G. Moruzzi 13, I-56124 Pisa, Italy.*

^b *Universidad de Burgos, Departamento de Química, Plaza Misael Bañuelos s/n, 09001 Burgos, Spain.*

^c *Dipartimento di Chimica Industriale “Toso Montanari”, Università di Bologna, Viale Risorgimento 4, I-40136 Bologna, Italy.*

^d *Dipartimento di Farmacia, Università di Pisa, Via Bonanno 6, I-56126 Pisa, Italy.*

Corresponding Authors

*E-mail addresses: fabio.marchetti1974@unipi.it; nbusto@ubu.es; lorenzo.biancalana@unipi.it

^a.

Abstract

Several complexes of general formula $[\text{Ru}(\text{halide})(\eta^6\text{-}p\text{-cymene})(\alpha\text{-diimine})]^+$, in the form of nitrate, triflate and hexafluorophosphate salts, including a newly synthesized iodide compound, were investigated as potential anticancer drugs and bactericides. NMR and UV-Vis studies evidenced remarkable stability of the complexes in water and cell culture medium. In general, the complexes displayed strong cytotoxicity against A2780 and A549 cancer cell lines with IC_{50} values in the low micromolar range, and one complex (**RUCYN**) emerged as the most promising one, with a significant selectivity compared to the non-cancerous HEK293 cell line. A variable affinity of the complexes for BSA and DNA binding was ascertained by spectrophotometry/fluorimetry, circular dichroism, electrophoresis and viscometry. The performance of **RUCYN** appears associated to enhanced cell internalization, favored by two cyclohexyl substituents, rather than to specific interaction with the evaluated biomolecules. The chloride/iodide replacement, in one case, led to increased cellular uptake and cytotoxicity at the expense of selectivity, and tuned DNA binding towards intercalation. Complexes with iodide or a valproate bioactive fragment exhibited the best antimicrobial profiles.

Keywords: ruthenium(II) arene complexes, α -diimine ligand, cytotoxicity, ruthenium cellular uptake, DNA binding, BSA interaction

Introduction

The research on prospective ruthenium-based drugs has been intensively carried out over the last 30 years, and some promising $\text{Ru}^{+\text{III}}$ and $\text{Ru}^{+\text{II}}$ complexes (NAMI-A, KP1019, NKP1339/IT-139 and TLD1433¹) have been investigated in clinical trials for cancer treatment.² In this setting, ruthenium(II) arene complexes have been widely studied,³ and the leading compound of this family, i.e. RAPTA-C (Scheme 1a), is currently undergoing a pre-clinical evaluation due to its notable antimetastatic,

antiangiogenic and antitumoral activity.⁴ A wide array of complexes has been screened for the anticancer activity *in vitro* and *in vivo*, and the attachment of a bidentate *N,N*-donor ligand to the Ru^{II}-arene skeleton has emerged as an advantageous structural feature.^{4,5} 1,2-Diamine complexes were among the first ones to be studied and especially RM175 [RuCl(ethylenediamine)(η^6 -biphenyl)]⁺ (PF₆⁻ salt; Scheme 1b) exhibited a potent activity against various cancer cell lines and also primary tumors.⁶ Within this framework, our interest has been focused on ruthenium(II) *p*-cymene complexes with α -diimines (Scheme 1c), which have been assessed for their cytotoxicity on 2D and 3D cancerous cell models.^{7,8}

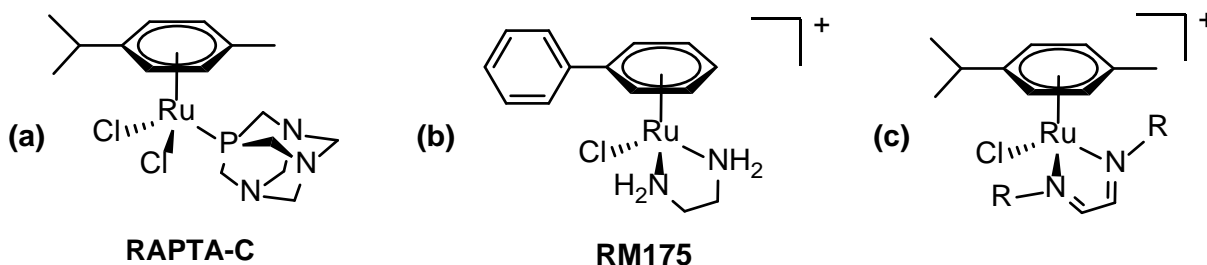


Figure 1. Ru^{II}(η^6 -arene) complexes with anticancer activity: structures of RAPTA-C(a), RM-175(b) and α -diimine complexes (c, R = aryl or alkyl).

Most of ruthenium(II)-arene complexes are viewed as *pro-drugs*, and it has been proposed that the dissociation of the chloride ligand in the physiological environment is key to activation, enabling the complex to interact with biosubstrates.^{4,5,9} The anticancer activity usually involves multiple intracellular targets, therefore elucidating the interaction of the complexes with biomolecules is of paramount importance.¹⁰

Albumins constitute the 60% of the total protein content of plasma¹¹ and are involved in the transport of many endogenous and exogenous compounds (drugs) through the blood.¹² Specifically, bovine serum albumin (BSA) is often employed as a model for experimental studies due to its cheapness, wide availability and similarity to human serum albumin (HSA).¹³

Besides serum proteins, DNA-drug interactions may be responsible for conformational changes of the polynucleotide, affecting its major functions.¹⁴ Over the past few years, an important amount of work has been published on the DNA binding ability of Ru^{+II} arene complexes.¹⁵ For instance, both RM-175 and RAPTA-C were shown by X-ray crystallography to form adducts by N-coordination of specific nucleobases of double-helical DNA, following chloride dissociation.¹⁶ On the other hand, complexes with extended aromatic ligands may establish non-covalent hydrophobic interactions with DNA, such as intercalation or groove binding.^{3a,17}

At variance to RM-175 and RAPTA-C, α -diimine complexes do not hydrolyze to a significant extent in aqueous solution,^{7a} the stability of the Ru-Cl bond being (in part) ascribable to the π -acceptor character of the α -diimine ligand.^{3a,7} In the light of the promising results from previous cytotoxicity studies and other favorable features (e.g., water solubility and stability, synthetic availability), we deemed worthwhile to expand the biological investigation on Ru^{+II} arene α -diimine complexes. Thus, a series of these compounds was selected to test the antiproliferative activity towards cancer and non-cancer cell lines, to determine the intracellular ruthenium uptake and to elucidate the interactions with potential biological targets such as DNA and BSA. An unprecedented complex with an iodide ligand (instead of chloride) is included in the present work, since this simple structural modification is expected to provide a significant effect. Actually, Ru^{+II}-arene iodido compounds show higher lipophilicity with respect to the chlorido analogues, resulting in better cell accumulation¹⁸ and possible enhanced cytotoxicity and selectivity.¹⁹ These features have been often associated to the higher inertness of the ruthenium-iodide bond compared to ruthenium-chloride.²⁰

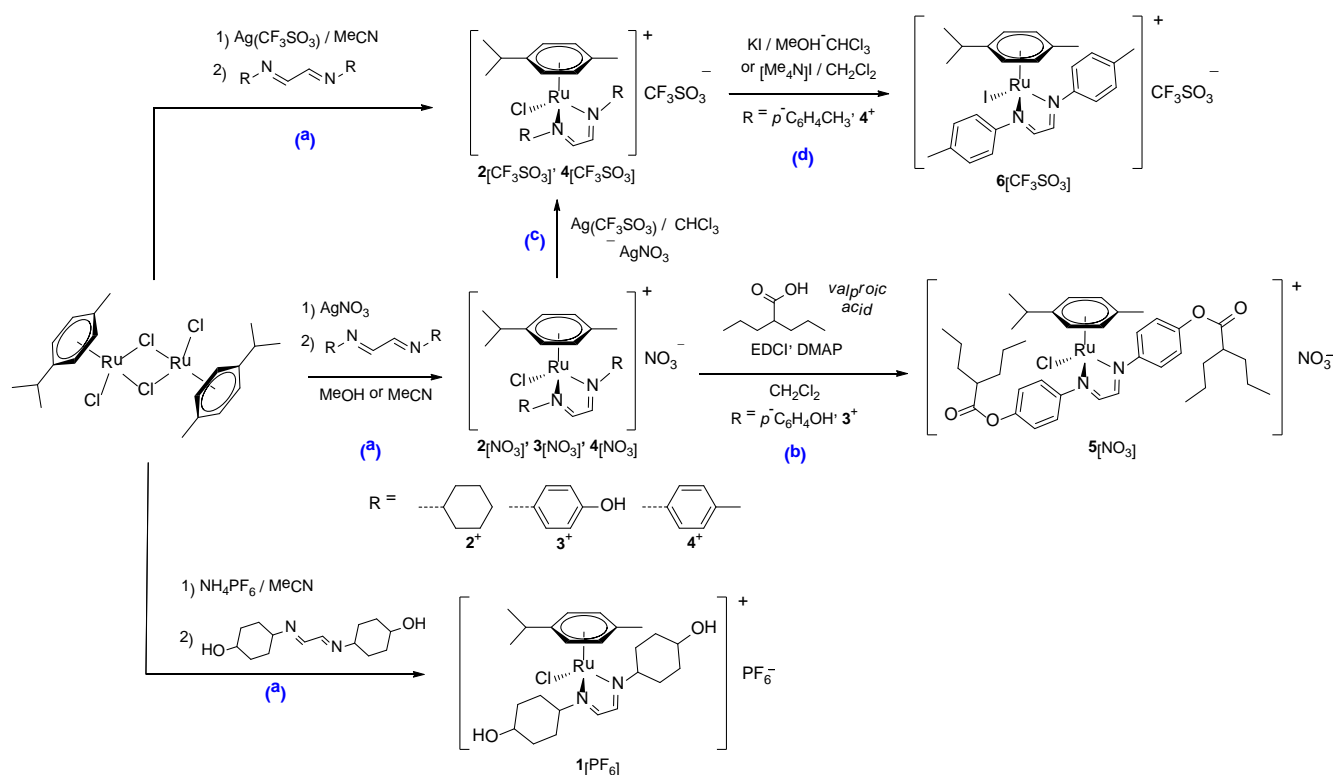
Furthermore, the antibacterial potential of the compounds was evaluated. Note that studies on the antibacterial activity of ruthenium(II) arene complexes are still scarce despite an increasing interest in the last few years.^{21,22}

Results and discussion

1. Synthesis and characterization of compounds.

Complexes $[\text{RuCl}(\eta^6\text{-}p\text{-cymene})\{\kappa^2N\text{-(HCN(4-C}_6\text{H}_{10}\text{OH))}_2\}][\text{PF}_6](\mathbf{1}[\text{PF}_6])$ and $[\text{RuCl}(\eta^6\text{-}p\text{-cymene})\{\kappa^2N\text{-(HCNR)}_2\}][\text{NO}_3]$ ($\text{R} = \text{C}_6\text{H}_{11}, \mathbf{2}^+; 4\text{-C}_6\text{H}_4\text{OH}, \mathbf{3}^+; 4\text{-C}_6\text{H}_4\text{CH}_3, \mathbf{4}^+$) were prepared from $[\text{RuCl}_2(\eta^6\text{-}p\text{-cymene})]_2$ and the respective α -diimine ligand (Scheme 1a), according to previously published procedures.⁷ Subsequent esterification of $\mathbf{3}[\text{NO}_3]$ with valproic acid afforded the bioactive-functionalized complex $\mathbf{5}[\text{NO}_3]$ (Scheme 1b).^{7a} Valproic acid is a histone deacetylase (HDAC) inhibitor²³ and its inclusion within metal-based scaffolds has been reported to be beneficial to the anticancer activity.^{7a,24} Moreover, valproic acid is capable of altering the biosynthesis of fatty acids and polyketides in microorganisms,²⁵ and its antimicrobial activity against *Mycobacterium tuberculosis* has been documented.²⁶

Next, aiming to introduce iodide as ligand, reactions of $\mathbf{2}[\text{NO}_3]$ and $\mathbf{4}[\text{NO}_3]$ with $\text{Ag}(\text{CF}_3\text{SO}_3)$ in refluxing chloroform were carried out. Nevertheless, the chloride ligands were not removed under these conditions, and only the anion-exchange products $\mathbf{2}[\text{CF}_3\text{SO}_3]$ and $\mathbf{4}[\text{CF}_3\text{SO}_3]$ were obtained (50% yield; Scheme 1c). The identity of the latter compounds was confirmed by direct synthesis from $[\text{RuCl}(\eta^6\text{-}p\text{-cymene})]_2/\text{Ag}(\text{CF}_3\text{SO}_3)$ and the α -diimine (98% yield; Scheme 1a), as well as by single crystal X-ray diffraction in the case of $\mathbf{4}[\text{CF}_3\text{SO}_3]$ (Figure 2). The molecular structure of the cation $\mathbf{4}^+$ was previously reported as NO_3^- salt,^{7b} showing almost identical geometry and bonding parameters. Subsequent treatment of $\mathbf{4}[\text{CF}_3\text{SO}_3]$ with potassium iodide or tetramethylammonium iodide afforded the desired $[\text{RuI}(\eta^6\text{-}p\text{-cymene})\{\kappa^2N\text{-(HCN(4-C}_6\text{H}_4\text{CH}_3))_2\}]\text{CF}_3\text{SO}_3$, $\mathbf{6}[\text{CF}_3\text{SO}_3]$ (82-88% yield; Scheme 1d). All new compounds $\mathbf{2}[\text{CF}_3\text{SO}_3]$, $\mathbf{4}[\text{CF}_3\text{SO}_3]$ and $\mathbf{6}[\text{CF}_3\text{SO}_3]$ were characterized by spectroscopic (IR, NMR) and analytical (CNH analysis, molar conductivity) techniques (see Experimental and Figures S1-S9).



Scheme 1. Preparation of ruthenium(II) arene α -diimine complexes: (a) α -diimine addition to $[\text{RuCl}_2(\eta^6\text{-}p\text{-cymene})]_2$; (b) esterification of α -diimine ligand; (c) nitrate/triflate anion metathesis; (d) chloride/iodide ligand exchange. **RUCYN** = 2[NO_3].

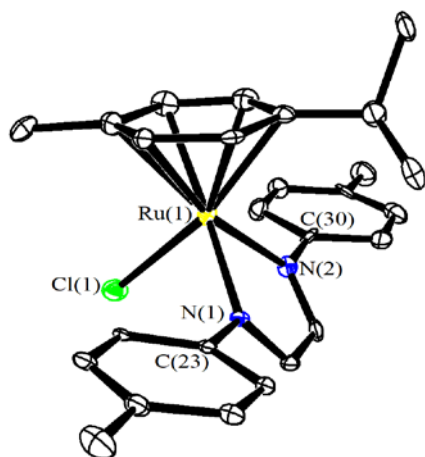


Figure 2. View of the molecular structure of the cation within 4[CF_3SO_3]. Displacement ellipsoids are at the 50% probability level. Hydrogen atoms are omitted for clarity. Main bond distances (\AA) and angles ($^\circ$): Ru(1)-N(1) 2.077(12), Ru(1)-N(2) 2.055(12), Ru(1)-Cl(1) 2.370(4), Ru(1)-($\eta^6\text{-}p\text{-cymene}$)_{av} 2.190(4), N(1)-Ru(1)-N(2) 75.8(5), N(1)-Ru(1)-Cl(1) 88.0(3), N(2)-Ru(1)-Cl(1) 86.9(3).

In view of the biological application, a detailed investigation on the behaviour of ruthenium α -diimine complexes in aqueous media was conducted. First, water solubility and octanol-water partition coefficients ($\text{Log } P_{\text{ow}}$) were assessed (Table 1). Compounds **1**[PF₆] and **2-4**[NO₃] possess an appreciable water solubility ($\geq 3 \text{ mM}$ in D₂O), instead the valproate diester **5**[NO₃] and the iodide **6**[CF₃SO₃] are hardly soluble in water. Remarkably, the solubility of the most performant anticancer compound (vide infra), i.e. **2**[NO₃] (**RUCYN**), is higher than that of cisplatin: approximate solubility values of **RUCYN** and cisplatin are respectively 5.5 and 3 g·L⁻¹.²⁷ Octanol-water partition coefficients of compounds featuring unsubstituted alkyl or aryl α -diimines (**2**[NO₃], **3**[NO₃] and **6**[CF₃SO₃]; $-0.6 < \text{Log } P_{\text{ow}} < +0.7$) evidence their *amphiphilic* character, while those derivatives with OH groups, i.e. **1**[PF₆] and **3**[NO₃], are more hydrophilic. Overall, the chloride/iodide exchange on going from **4**⁺ to **6**⁺ (and parallel NO₃⁻/CF₃SO₃⁻ exchange) led to a decrease in water solubility and dramatic increase in lipophilicity.

Table 1. Solubility in water (D₂O) and octanol/water partition coefficient ($\text{Log}_{10} P_{\text{ow}}$) of Ru compounds.

Compound	D ₂ O solubility ^[a] (21°C)/ mol·L ⁻¹	Partition coefficient ($\text{Log}_{10} P_{\text{ow}}$)
1 [PF ₆]	$9.9 \cdot 10^{-3}$	-1.38 ± 0.05
2 [NO ₃]	$1.0 \cdot 10^{-2}$	-0.63 ± 0.04
3 [NO ₃]	$5.6 \cdot 10^{-3}$	-0.91 ± 0.05
4 [NO ₃]	$3.1 \cdot 10^{-3}$	-0.68 ± 0.02
5 [NO ₃]	$< 10^{-4}$ ^[b]	> 2.5
6 [CF ₃ SO ₃]	$< 10^{-4}$ ^[b]	0.71 ± 0.03

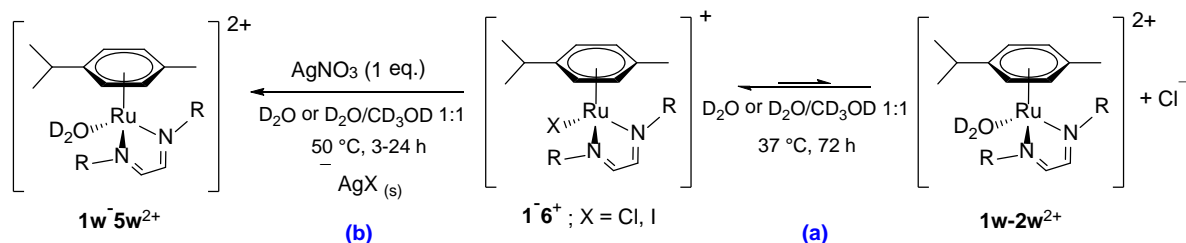
[a] Solubility data for **1**[PF₆] and **2-4**[NO₃] were taken from the literature.^{7b} [b] Below the lowest value of quantitation.

Next, the stability and speciation in aqueous solution was investigated by ¹H NMR spectroscopy (Table 2; Figures S10-S15). Thus, D₂O (or D₂O/CD₃OD) solutions of **1**⁺-**6**⁺ were incubated at 37°C for 72 h and a considerable fraction (88-98 %) of the starting material was detected at the end of the experiment in every case. In the case of **1**⁺ and **2**⁺, a second set of ¹H NMR signals appeared, which we attributed to the respective aquo-complexes [Ru(D₂O)(η^6 -*p*-cymene)(α -diimine)]²⁺ (**1w**²⁺ and **2w**²⁺, Scheme 2a).

Subsequently, solutions of 1^+-6^+ were treated with AgNO_3 (1 eq) and kept at 50°C for a variable time (3-24 h). Despite no reaction occurred initially, formation of the aquo complexes was later recognized ($1w^{2+}$ - $5w^{2+}$; Scheme 2b). This experiment allowed unambiguous assignment of the ^1H NMR set of signals for halido and aquo complexes, thus confirming that $[\text{RuX}(\eta^6\text{-}p\text{-cymene})(\alpha\text{-diimine})]^+$ complexes ($\text{X} = \text{Cl}, \text{I}$) are not easily hydrolysed in aqueous solution.^{7a} Interestingly, complexes bearing aliphatic α -diimine ligands (1^+-2^+) are much more inert towards Ag^+ -driven halide displacement than those bearing N -aryl groups ($4^+, 5^+, 6^+$; with 3^+ as a special case, *vide infra*), as opposed to the behaviour in pure water.

Furthermore, the stability of 1^+-4^+ and 6^+ in deuterated cell culture medium ("DMEM-d") over 24 h at 37°C was assessed by ^1H NMR (Table 2). All complexes showed a substantial robustness (stability ≈ 75 -90 %) and no hydrolysed species ($1w^{2+}$ - $4w^{2+}$) were detected. Therefore, both the chlorido (4^+) and the iodido (6^+) derivatives retain their molecular identity under such challenging conditions. No evidence was collected to any extent for iodido/chlorido exchange in 6^+ , despite the high Cl^- concentration in the cell culture medium ($\approx 0.11\text{ M}$). These results outline a remarkable robustness of the $\text{Ru}(\text{arene})(\alpha\text{-diimine})$ scaffold, which is a fundamental preliminary property in the view of biological applications. Otherwise, the stability of 5^+ in the cell culture medium was prevented by the insolubility of this complex, however the cell uptake experiments suggest the occurrence of ester bond cleavage to some extent (*vide infra*).

Table 2/Scheme 2. Stability of ruthenium compounds in D_2O or cell culture medium by ^1H NMR. Hydrolysis after 72 h at 37°C (a) or following 3 h or 24 h treatment with AgNO_3 at 50°C (b).



Compound	Solvent	% stability ^[a]	% hydrolysis ^[b]			Solvent	% stability ^[a]
		72 h, 37 °C	72 h, 37 °C	+ AgNO ₃ 1 eq. 3 h, 50 °C	24 h, 50 °C		24 h, 37 °C
1 [PF ₆]	D ₂ O	88	8.5 %	11 %	45 %	DMEM-d	91
2 [NO ₃]	D ₂ O	91	6.5 %	12 %	40 %	DMEM-d	94
3 [NO ₃]	D ₂ O:CD ₃ OD 7:1	99	<i>n.d.</i>	2 %	14 %	DMEM-d:CD ₃ OD 7:1	79
4 [NO ₃]	D ₂ O:CD ₃ OD 7:1	98	<i>n.d.</i>	55 % ^[c]	85 % ^[c]	DMEM-d: CD ₃ OD 7:1	75
5 [NO ₃]	D ₂ O:CD ₃ OD 1:1	93	<i>n.d.</i>	> 80 % ^[d]	-	DMEM-d: CD ₃ OD 1:1	-
6 [CF ₃ SO ₃]	D ₂ O:CD ₃ OD 1:1	94	<i>n.d.</i>	100 %	-	DMEM-d: CD ₃ OD 1:1	75

n.d. = not detected. [a] Relative amount with respect to the initial spectrum of the starting material, Me₂SO₂ as internal standard. [b] Molar ratio vs. starting material. [c] An additional, transient complex is observed at 3 h; multiple species are present at 24 h. [d] Formation of a brown solid.

UV-Vis spectroscopic characterization in aqueous buffer solution (NaCl 0.1 M, NaCac 2.5 mM, pH 7.0) revealed that all complexes display metal-to-ligand charge-transfer bands in the 300-500 nm range,^{7a} with lower molar extinction coefficients for **1**⁺-**2**⁺ lacking extended π system (Figure S16, Table S1). Complex **3**⁺, containing the *N*-phenol group, is blue-shifted compared to other *N*-aryl complexes (**4**⁺ and **6**⁺), and it is the highest visible-absorbing species, also displaying an additional band at 580 nm. The profile of the UV-vis spectrum of **3**⁺ is pH-dependent (Figure S17), due to the deprotonation of the OH group, for which a pK_a value of 7.7 \pm 0.1 (0.1 M NaCl) had been determined.^{7a} Given that in the present work we used also low salt content conditions, we repeated the evaluation in the absence of NaCl. Spectroscopic data were analysed by the HypSpec2014® software (Figure S18) and confirmed the presence of a single equilibrium with pK_a = 8.0 \pm 0.1. The two values turn to be fully in agreement when one is converted into the other by means of the Davies equation for salt effects.²⁸ Therefore, at physiological pH, *ca.* 90% of the complex is present in its original non-dissociated form.

2. Biological studies.

Cytotoxicity. The cytotoxicity of all complexes, and of cisplatin (cPt) as a reference, was tested through the MTT assay after 72 h of incubation. The tested cell lines are those of human ovarian carcinoma (A2780), human lung carcinoma (A549) and healthy human embryonic kidney (HEK293).

In order to elucidate if the interaction of the studied complexes with serum proteins influences their availability and, consequently, their cytotoxicity,²⁹ the activity against the cellular line A549 was tested using both the standard serum-supplemented medium (10% FBS) and the serum-deprived medium (1% FBS). Table 3 collects the obtained half maximal inhibitory concentrations (IC_{50} values) from the survival curves (Figure S19).

Table 3. IC_{50} values (μM) determined for complexes on human lung carcinoma (A549), human ovarian carcinoma (A2780), and healthy human embryonic kidney (HEK293) cells after 72 hours incubation for Ru compound and cisplatin (cPt). Values are given as the mean \pm SD.

Compound	IC_{50} , μM			
	A549	A549 (1% FBS)	A2780	HEK293
1 [PF ₆]	n.e. ^[a]	> 50	> 50	> 50
2 [NO ₃]	4.3 \pm 0.6	6.1 \pm 0.8	2.3 \pm 0.3	10.7 \pm 1.0
3 [NO ₃]	n.e. ^[a]	> 50	> 50	n.e. ^[a]
4 [NO ₃]	15.7 \pm 1.2	12.9 \pm 1.8	49.2 \pm 3.1	2.6 \pm 0.4
5 [NO ₃]	5.8 \pm 0.8	4.1 \pm 0.6	5.3 \pm 0.3	6.9 \pm 0.8
6 [CF ₃ SO ₃]	2.7 \pm 0.2	3.5 \pm 0.6	6.5 \pm 0.6	0.23 \pm 0.04
cPt	3.8 \pm 0.6	4.8 \pm 0.3	2.6 \pm 0.3	4.4 \pm 0.6

[a] n.e.= no effect was observed throughout the tested concentration range (0-50 μM).

Complexes **2**⁺, **5**⁺ and **6**⁺ show a comparable level of antiproliferative activity towards the two cancer cell lines and the IC_{50} values close those obtained for cisplatin. Complex **4**⁺ is less cytotoxic, especially against the A2780 cells, while **1**⁺ and **3**⁺ are not cytotoxic, evidencing that the presence of hydroxyl groups on the α -diimine ligand is detrimental to the activity. In general, the activity does not seem to be influenced by the serum proteins concentration. The complexes are non-selective towards the cancer cells compared to the non-cancerous cell line, except **2**⁺ showing some selectivity. The introduction of the valproate (VP) bioactive fragment in **5**⁺ provides an increased antiproliferative activity compared to **3**⁺ and **4**⁺, although it does not appear to contribute to selectivity. The results obtained for **1**⁺-**3**⁺ and **5**⁺ against A2780 and HEK-293 cell lines are in alignment with previous findings.^{7a} It is noteworthy

that, moving from the chloride 4^+ to the iodide analogue 6^+ , the cytotoxicity increased in all cell lines. This may be related to the strong enhancement of the lipophilicity (Table 1) and, consequently, to the cellular uptake (see below). However, a negative impact on the selectivity is noticed.

The biological activity of the Ru^{+II} complexes against the A549 cells was corroborated by microscopy visualization after 24 h of treatment. The A549 cells in normal conditions appear with a long fusiform shape, small size and clear cell boundaries³⁰ (see 1^+ and 3^+ inactive compounds, Figure S20). Concerning the cytotoxic compounds, morphological changes appear around the IC_{50} concentration (5 μM for 2^+ , 5^+ and 6^+ and 10 μM for 4^+ , Figure S20), being more evident when the drug concentration is raised. The rounding of the cell body and the formation of neurite-like projection indicate the blebbing of the plasma membrane and is compatible with apoptosis.³¹

Cell uptake. The uptake of the complexes in A549 cells was determined by ICP-MS after 24h of incubation at 2 μM of each complex. Cisplatin was included for comparison and RAPTA-C, which is known to exert its functions mainly outside the cell environment, was evaluated as a reference ruthenium compound. The results are shown in Figure 3.

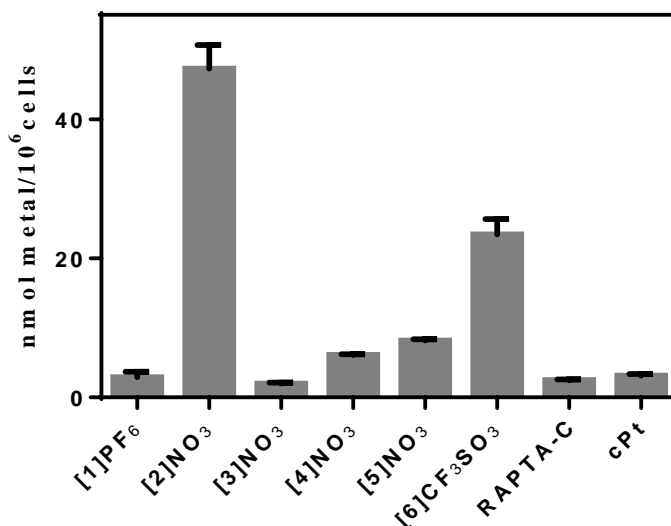


Figure 3. ICP-MS results showing metal accumulation in A549 cells after 24 h of exposure to 2 μ M of complexes. Results (mean and SD) are expressed as nanomols of metal in one million cells.

In general, the results are in good agreement with the cytotoxicity data and the complexes result more internalized than cPt and RAPTA-C. Moreover, there is a parallelism between the increasing cellular internalization and the lipophilicity of the organometallic cation, ongoing along the series $\mathbf{1}^+$ (N-cyclohexanol group) < $\mathbf{3}^+$ (N-phenol) to $\mathbf{4}^+$ (N-tolyl) and then $\mathbf{6}^+$ (N-tolyl and iodide ligand). Complex $\mathbf{5}^+$ is only limitedly internalized despite the high lipophilicity imparted by the valproate fragments ($\text{Log } P_{\text{ow}} > 2.5$ for $[\mathbf{5}]\text{NO}_3$), therefore it seems plausible that esterolysis of the valproate occurs to some extent outside the cancer cells from $\mathbf{5}^+$ (vide infra). An exceptional ruthenium internalization was measured following incubation with complex $\mathbf{2}^+$, that was not expected looking at the partition coefficient ($\text{Log } P_{\text{ow}} = -0.63$ for $[\mathbf{2}]\text{NO}_3$). The favorable effect on the anticancer activity provided by the decoration of metal complexes, including ruthenium-arene complexes, with a cyclohexyl group was previously recognized in the literature in a few cases. It was suggested that the compact and hydrophobic cyclohexyl could facilitate the crossing of cell membrane and thus the entrance of the metal complex into the tumor cell.³²

Antimicrobial activity.

The antibacterial activity of the complexes was evaluated by the microdilution method in four pathogenic bacteria of clinical interest. Two Gram-positive (vancomycin-resistant *Enterococcus faecium* and a methicillin-resistant *Staphylococcus aureus*) and two Gram-negative (*Acinetobacter baumannii* and *Pseudomonas aeruginosa*) strains were included. The minimal inhibitory concentrations (MIC) are collected in Table 4. Complexes **1**⁺-**3**⁺ are completely inactive or display no significant activity, while **4**⁺ shows a moderate activity against Gram+ bacteria being completely inactive against Gram- strains. Moreover, the hydrophobic cations (see Log *P*_{ow} values in Table 1) **5**⁺ and **6**⁺ are highly active against Gram+ strains whereas only **6**⁺ is active against Gram- bacteria. As previously observed for the cytotoxicity, the introduction of the iodide ligand enhances the antibacterial potential and seems to be the key for the antimicrobial activity against Gram- bacteria.

Table 4. MIC values (the lowest concentration of the compound that prevents bacterial growth) of the studied compounds.

Compound	MIC, μM			
	<i>E. faecium</i>	<i>S. aureus</i>	<i>A. baumannii</i>	<i>P. aeruginosa</i>
1 [PF ₆]	>80	> 80	> 80	> 80
2 [NO ₃]	80	40	> 80	> 80
3 [NO ₃]	80	40	> 80	> 80
4 [NO ₃]	20	20	> 80	> 80
5 [NO ₃]	1.3	0.3	80	> 80
6 [CF ₃ SO ₃]	0.6	0.3	10	20

Interaction with Bovine serum albumin (BSA). In order to check the possible BSA interaction of complexes **1**⁺-**4**⁺, spectrofluorometric titrations at 25°C were performed, by adding increasing amounts

of the ruthenium complexes to the fluorescent protein. A fluorescence emission decrease upon addition of the tested complexes was detected (Figures 4A and S21).

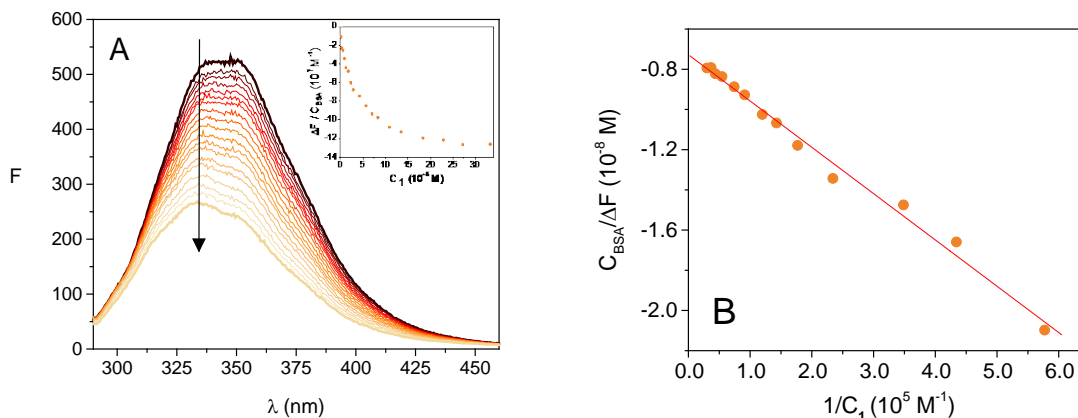


Figure 4. (A) Spectrofluorimetric titration of BSA with 1^+ (inset: binding isotherm) and (B) relevant plot according to Eq.(1); $C_{BSA} = 1.52 \times 10^{-6}$ M, $C_1 = 0 - 3.3 \times 10^{-5}$ M, NaCl 0.1 M, NaCac 2.5 mM, pH 7.0, DMSO_{max} 0.1 %, 25.2 °C.

The Stern-Volmer constants (K_{SV}) for all studied systems were determined through the modified Stern-Volmer equation (Figure S22, Table S2). K_{SV} do not significantly increase with temperature and its order of magnitude is $10^5 \text{ M}^{-1} \text{ s}^{-1}$: these results are in agreement with adduct formation.³³ The equilibrium constant for the binding process (K) was determined by equation (1), (see “Methods” section, Figures 4B and S23, and Table S2).

$$\frac{C_{BSA}}{\Delta F} = \frac{1}{K \Delta \phi} + \frac{1}{[i]} + \frac{1}{\Delta \phi} \quad (1)$$

Here, C_{BSA} is the total molar concentration of BSA, $[i]$ is the molar concentration of the free tested ruthenium complex and $\Delta \phi = \phi_{\text{boundBSA}} - \phi_{\text{unboundBSA}}$ is the change in the optical parameters, being under these diluted conditions $F_i = \phi_i [i]$; note that the exact calculation of $[i]$ requires an iterative procedure.³³ The K values for BSA interaction agree with previous data on the interaction of related complexes with albumins.³⁴ The binding process was further analyzed by circular dichroism (CD) experiments, which enable a better enlightenment of the possible binding-induced conformational

changes in the protein. CD spectra of BSA were recorded both in the absence and in the presence of a 5-fold excess of the complexes. Since none of the complexes display a CD signal in buffer, the observed changes in the molar ellipticity of the protein along with the (slight) blue-shifts found for **1**⁺ and **4**⁺ show that these complexes are able to induce a variation in the CD band of BSA (Figure 5).

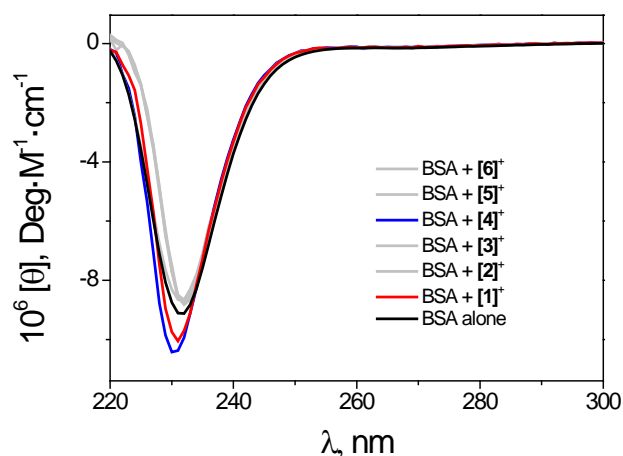


Figure 5. CD spectra of BSA alone and in the presence of the complexes under study. $C_{\text{BSA}} = 0.5 \mu\text{M}$, $C_{\text{complexes}}/C_{\text{BSA}} = 5$, NaCl 0.1 M, NaCac 2.5 mM, pH 7.0, DMSO 0.0025% and $T = 25^\circ\text{C}$.

This result is further confirmed by native polyacrylamide gel protein (PAGE) electrophoresis experiments after overnight incubation at 37.0°C of **1**⁺-**6**⁺/BSA mixtures (Figure 6). BSA alone and BSA in the presence of the maximum DMSO concentration used in the experiments were included as negative controls. It was found that **1**⁺ and **4**⁺ (at the higher concentration) are the species which seem to affect the protein conformation. For all the other complexes, no variation was observed in the electrophoretic mobility of native BSA. ~~The potentiality of the non-cytotoxic complex **1**⁺ to interact with proteins deserves some more comment. It is well documented that RAPTA-C, a leading ruthenium anticancer drug candidate, is substantially not cytotoxic and exerts its action prevalently by targeting specific proteins.⁴ Therefore, it is possible that **1**⁺ holds a potential as anticancer drug despite its inactivity in 2D in vitro trials, although more advanced studies would be needed to deepen this point.~~

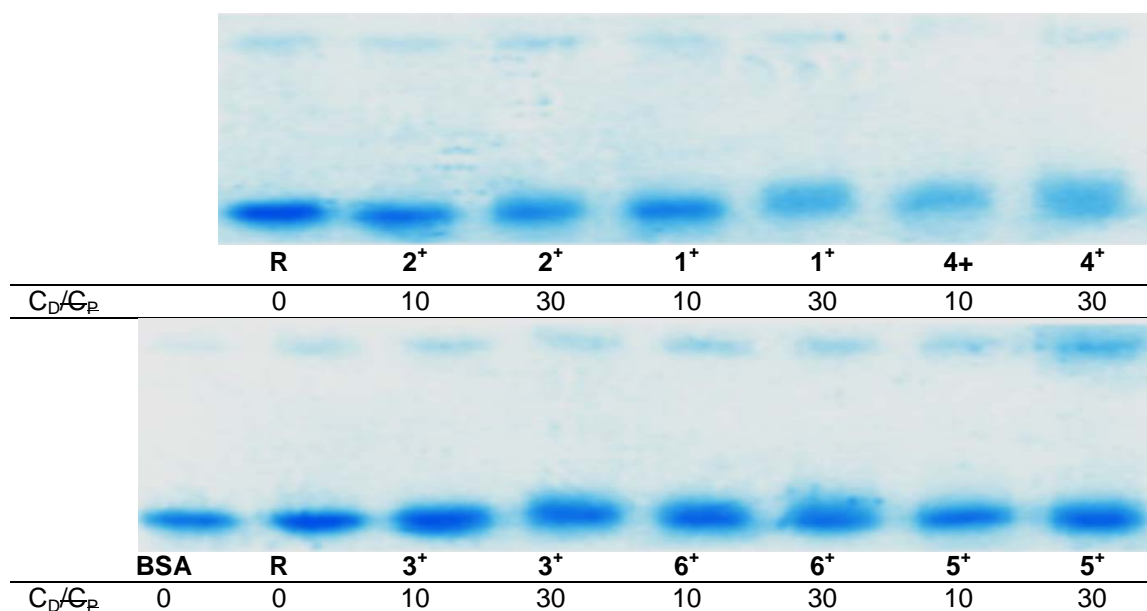


Figure 6. Native acrylamide electrophoresis of BSA incubated overnight with Ru complexes at 37 °C, $C_{complex}/BSA = C_D/C_P = 10$ and 30. $C_P = 1 \mu M$, $C_D = 10$ and $30 \mu M$. (BSA = BSA alone, R = vehicle control (BSA with 0.03% DMSO)). NaCl 0.1 M, NaCac 2.5 mM, pH 7.0.

Interaction with DNA. The interaction of the complexes with plasmid DNA (pUC18) was studied by means of agarose gel electrophoresis tests for [complex]/[DNA] (C_D/C_P) between 0 and 5.0 and using cisplatin (**cPt**) as positive control for covalent binding (buffer NaCac 2.5 mM at pH 7.0)(Figure 7). It is found that **3⁺** and **4⁺** are the only species which can change the migration behavior of the SC conformation of the polynucleotide. For **3⁺** and **4⁺**, the migration rate of the SC band decreases as the concentration of the complex is increased, similarly to the **cPt** behavior, suggesting an interaction which significantly alters DNA conformation. By contrast, the other complexes are not able to induce such conformational changes in DNA structure.

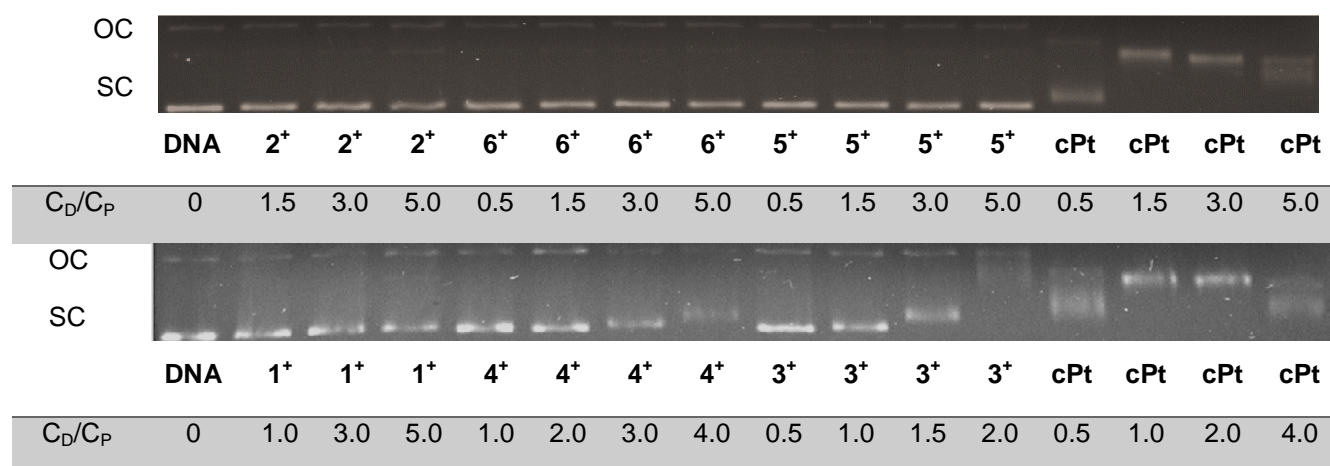


Figure 7. Agarose gel electrophoresis of plasmid DNA (OC = open circular conformation; SC = supercoiled conformation) incubated overnight at 37 °C with the different ruthenium complexes at several [complex]/[DNA] (C_D/C_P) ratios. $C_{pDNA} = 0.37 \mu M$, NaCac 2.5 mM, DMSO 0.2 %. $t_{run} 2.30$ h, 6.5V/cm, EtBr staining.

Kinetic tests were then performed, where the absorbance profile evolution in time was recorded. When solid **3⁺** and **4⁺** were directly dissolved in water or in DMSO no spectral variation was observed, according to NMR experiments. When DNA was added to a mixture of **3⁺** dissolved in H₂O, a spectral time-dependence was recognized (Figure 8A). The same for **4⁺** (Figure 8B). Overall, the presence of this slow kinetic effect confirms that **3⁺** and **4⁺** are able to progressively induce significant DNA conformational changes, suggesting the establishment of a covalent interaction.

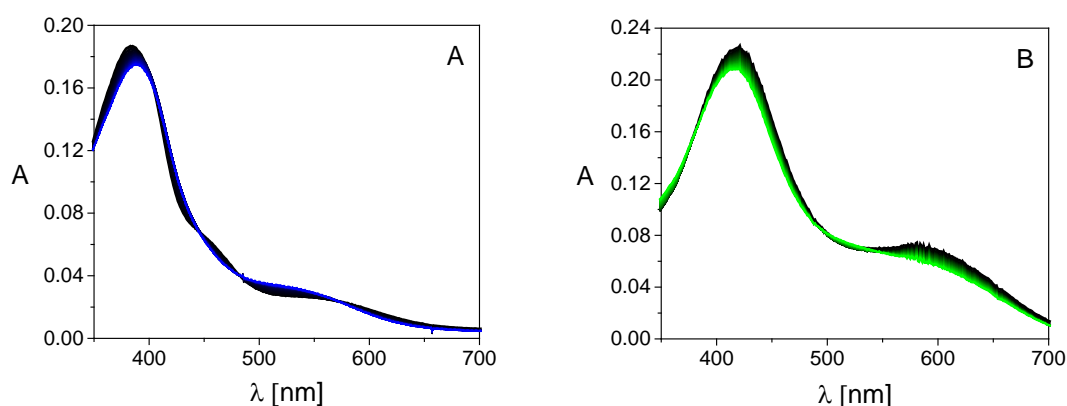


Figure 8. Absorption spectra evolution in time (5h) of a mixture of DNA with **3⁺** (A) or **4⁺** (B) in NaCac 2.5 mM at pH 7.0, 25.0 °C, DMSO 0.25%.

Ethidium Bromide (EtBr) displacement assays were done, where the tested species is added to DNA saturated by EtBr. No significant variations of the probe signal are observed in the case of **1**⁺ and **2**⁺. By contrast, with **3**⁺ and **4**⁺ (both bearing an aromatic residue), some decrease of the emission intensity of EtBr was observed upon increasing addition of the tested complex (Figure S24). This suggests the presence of an interaction able to disturb EtBr from its intercalated position. Direct spectrophotometric titrations of **3**⁺ and **4**⁺ further confirmed the interaction features: successive additions of DNA to the complex solutions resulted in a hypochromic effect (Figure S25). The steep binding isotherms of **3**⁺ and **4**⁺ agree with quantitative binding to DNA (no binding constant could be calculated); this finding agrees with covalent binding. For **5**⁺, the spectroscopic features are not so favorable, still no binding reaction could be evidenced. Interestingly, also titrations of **6**⁺ showed positive results (Figure S25) with strong hypochromic and bathochromic effects ($\Delta\lambda = 5$ nm) which indicated that **6**⁺ interacts with DNA differently from **3**⁺ and **4**⁺. The non-quantitative binding between DNA and **6**⁺ has been studied at different temperatures and the relevant binding constants were calculated (see “Methods” section).³⁵

$$\frac{C_P(C_D\Delta\epsilon - \Delta A)}{\Delta A} = \frac{1}{nK} + \frac{(C_D\Delta\epsilon - \Delta A)}{\Delta\epsilon} \frac{1}{n} \quad (2)$$

$$\frac{C_P}{\Delta F} = \frac{1}{K\Delta\phi} + \frac{1}{C_P f(r)} + \frac{1}{\Delta\phi} \quad (3)$$

where $C_P = C_{DNA}$, $C_D = C_{complex}$, K is the binding constant, $f(r) = (1 - nr)^n / [1 - (n-1)r]^{n-1}$, $r = \Delta F / (\Delta\phi C_P)$ and n corresponds to the site size. Figure S26 shows the relevant fitting plots and Table 5 collects the results.

Table 5. Binding constant (K) and site size (n) for the DNA/**6**⁺ system at different temperatures. NaCac 2.5 mM, pH 7.0.

T (°C)	K (10 ⁴ M ⁻¹)	n
--------	--------------------------------------	---

25.0	6.1 ± 0.5	2.6
37.0	3.6 ± 0.3	2.2
47.0	2.5 ± 0.3	2.0

The order of magnitude of the K values agree with both groove binding and intercalation. Minor groove binders bearing an analogous structure, such as $[\text{RuCl}(\kappa^2\text{-}N,N\text{-}2\text{-pydaT})(\eta^6\text{-}p\text{-cymene})]\text{BF}_4$ (2,4-diamino-6-(2-pyridyl)-1,3,5-triazine,³⁶ $[\text{RuCl}(2\text{-pypzdp})](\eta^6\text{-C}_6\text{H}_6)]$ (pypzdp = 5-(2-pyrimidyl)piperazine)phenyldipyrromethane and $[(\eta^6\text{-C}_{10}\text{H}_{14})\text{RuCl}(2\text{-pmpzdp})]$, (pmpzdp = 5-(2-pyridyl)piperazine)phenyldipyrromethane)³⁷ do bind DNA with $K = 10^4 - 10^5$. On the other hand, even if the values in Table 5 are tenfold lower than those found for Ru(II) intercalators with extended aromatic ligands,³⁸ species such as $[\text{RuCl}(N\text{-methylhomopiperazine})(\eta^6\text{-C}_6\text{H}_6)]$ and $[\text{RuCl}(\text{L})(\eta^6\text{-arene})]$ (arene = C_6H_6 , p -cymene, $\text{L} = 1\text{-(anthracen-10-ylmethyl)-4-methylhomopiperazine}$) yielded DNA intercalation constants which also lie in the $10^4 - 10^5$ range.³⁹ The thermodynamic parameters may provide a signature which helps to fix the binding mode for the DNA/ $\mathbf{6}^+$ system: their indicative values were determined through a Van't Hoff plot (Figure S27) which yielded $\Delta H = -32 \text{ kJ mol}^{-1}$ and $\Delta S = -17 \text{ J mol}^{-1} \text{ K}^{-1}$. These values are again consistent with both groove binding and partial intercalation.⁴⁰ Viscometric experiments were conducted on the complexes which showed DNA binding features ($\mathbf{3}^+$, $\mathbf{4}^+$ and $\mathbf{6}^+$). The different solutions of DNA with the compounds were prepared and incubated overnight. The DNA viscosity does not change much in the presence of $\mathbf{3}^+$ and $\mathbf{4}^+$, this behavior being consistent with a covalent bond DNA-complex; on the contrary, increasing amounts of $\mathbf{6}^+$ lead to a viscosity enhancement (Figure S28). The latter finding enables to conclude that partial intercalation is the binding mode for the DNA/ $\mathbf{6}^+$ system. Again, the presence of iodide significantly changes the biological effects of the metal complex. The different DNA binding mode is often related to different aquation/hydrolysis processes at work,⁴¹ which is not the present case, since both $\mathbf{3}^+$, $\mathbf{4}^+$ and $\mathbf{6}^+$ do not hydrolyze to a significant extent (Table 2). However, solvent effects and hydrophobicity may also tune the binding mode.⁴² Therefore, it may be speculated that the much higher lipophilicity of $\mathbf{6}^+$ respect to

the **3**⁺ and **4**⁺ counterparts (Table 1) plays a major role in driving the penetration of **6**⁺ inside the hydrophobic DNA helix, also hindering possible covalent bonding.

Conclusions

Ruthenium(II) arene complexes have been extensively investigated as anticancer drug candidates, and recent studies evidenced the promising potential of α -diimine derivatives, combined with favorable characteristics such as easy availability, water solubility and stability in aqueous solutions. Here, we report further cytotoxicity assays on a series of Ru^{II}-arene- α -diimine complexes, and a detailed investigation aimed to clarify their mode of action. The results point out that changes in the nature of the diimine substituent may produce significant (but not easy to rationalize) effects on the antiproliferative activity and on the binding with BSA (investigated as a model protein) and DNA. The introduction of an iodide ligand in the place of chloride determines profound consequences on the activity, which seem ascribable to the increased lipophilicity and a change in the mode of interaction with DNA, rather than to a different hydrolytic behavior. One complex of the series (**RUCYN**) emerges as the most promising drug candidate: when compared to cisplatin, **RUCYN** exhibits higher water solubility, comparable cytotoxicity and higher selectivity with respect to a noncancerous cell line. This performance appears related to the presence of two cyclohexyl substituents, leading to a striking cell uptake, and it does not parallel to significant BSA/DNA binding, suggesting that further studies will be needed to unveil the possible targets and pathways for this species. Finally, the complexes were investigated for their antibacterial potential, the obtained results are promising and evidence the favorable roles of the valproate fragment and the iodide ligand.

Experimental

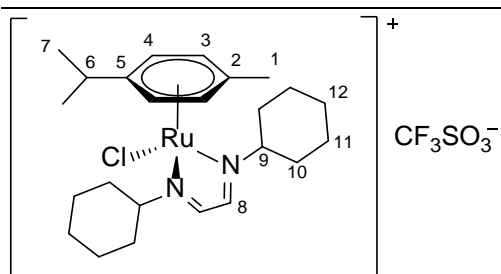
1. General experimental details.

All reagents and solvents were obtained from Alfa Aesar, Sigma Aldrich or TCI Europe and were used without further purifications. Compounds $[\text{RuCl}(\eta^6\text{-}p\text{-cymene})(\kappa^2N\text{-}\{\text{HCN}(4\text{-C}_6\text{H}_{10}\text{OH})_2\})][\text{PF}_6]$, **1** $[\text{PF}_6]$, $[\text{RuCl}(\eta^6\text{-}p\text{-cymene})\{\kappa^2N\text{-}(\text{HCN}(\text{C}_6\text{H}_{11}))_2\}][\text{NO}_3]$, **2** $[\text{NO}_3]$, $[\text{RuCl}(\eta^6\text{-}p\text{-cymene})\{\kappa^2N\text{-}(\text{HCN}(4\text{-C}_6\text{H}_4\text{OH}))_2\}][\text{NO}_3]$, **3** $[\text{NO}_3]$, $[\text{RuCl}(\eta^6\text{-}p\text{-cymene})\{\kappa^2N\text{-}(\text{HCN}(4\text{-C}_6\text{H}_4\text{CH}_3))_2\}][\text{NO}_3]$, **4** $[\text{NO}_3]$, $[\text{RuCl}(\eta^6\text{-}p\text{-cymene})\{\kappa^2N\text{-}(\text{HCN}(4\text{-C}_6\text{H}_4\text{OCOCH}^n\text{Pr}_2))_2\}][\text{NO}_3]$, **5** $[\text{NO}_3]$ and *N,N*-bis(4-methylphenyl)ethylenediamine were prepared according to literature methods.^{7,43} The synthesis of **5** $[\text{NO}_3]$ was carried out under a N_2 atmosphere using standard Schlenk techniques and CH_2Cl_2 distilled from P_2O_5 ; all the other operations were conducted in air with common laboratory glassware. Ru complexes were isolated as air- and moisture-stable solids and were stored at room temperature. NMR spectra were recorded on a Bruker Avance II DRX400 instrument equipped with a BBFO broadband probe at 25°C, unless otherwise specified. Chemical shifts (expressed in parts per million) are referenced to the residual solvent peaks⁴⁴ (^1H , ^{13}C) or to external standard (^{19}F to CFCl_3).⁴⁵ Infrared spectra of solid samples were recorded on a Perkin Elmer Spectrum One FT-IR spectrometer, equipped with a UATR sampling accessory. IR spectra were processed with Spectragryph software.⁴⁶ Carbon, hydrogen and nitrogen analyses were performed on a Vario MICRO cube instrument (Elementar). Conductivity measurements were carried out at 21 °C using an XS COND 8 instrument (cell constant = 1.0 cm^{-1}).⁴⁷

2. Synthesis and characterization of ruthenium compounds.

$[\text{RuCl}(\eta^6\text{-}p\text{-cymene})\{\kappa^2N\text{-}(\text{HCN}(\text{C}_6\text{H}_{10}))_2\}][\text{CF}_3\text{SO}_3]$, **2** $[\text{CF}_3\text{SO}_3]$ (Chart 1)

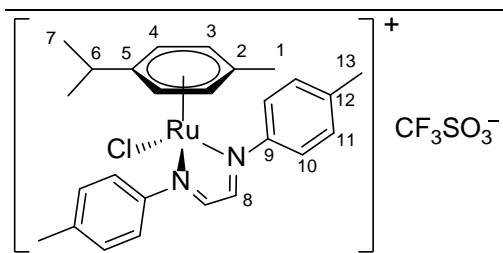
Chart 1. Structure of **2** $[\text{CF}_3\text{SO}_3]$ (numbering refers to carbon atoms).



A solution of **2**[NO₃] (76 mg, 0.14mmol) in CHCl₃ (8 mL) was treated with Ag(CF₃SO₃) (37 mg, 0.14mmol) and stirred at reflux temperature under protection from the light. After 3 h, an orange-brown solution and colorless solid (AgNO₃) were obtained. The mixture was filtered over a celite pad and the filtrate was dried under vacuum. The residue was triturated with Et₂O and the suspension was filtered. The resulting orange-brown solid was thoroughly washed with Et₂O and dried under vacuum (40 °C). Yield: 44 mg, 50 %. Compound **2**[CF₃SO₃] is soluble in MeOH, CH₂Cl₂, CHCl₃, insoluble in Et₂O. Anal. Calcd. For C₂₅H₃₈ClF₃N₂O₃RuS: C, 46.90; H, 5.98; N 4.38. Found: 46.70; H, 6.05; N, 4.33. IR (solid state): $\tilde{\nu}/\text{cm}^{-1}$ = 3069w, 3013w, 2935m, 2859w, 1628br, 1538w ($\nu_{\text{C}=\text{N}}$), 1471w, 1453w, 1106w, 1391-1349w, 1271s-sh ($\nu_{\text{S}=\text{O}}$), 1257s ($\nu_{\text{S}=\text{O}}$), 1223s-sh, 1154s, 1091w, 1075w, 1054w, 1028s ($\nu_{\text{S}=\text{O}}$), 913w, 871w, 749s, 666m. Λ_{m} (MeOH, $c = 1.0 \cdot 10^{-3}$ M) = 98 S·cm²·mol⁻¹. ¹H NMR (CDCl₃): δ/ppm = 8.25 (s, 2H, C8-H), 5.78 (d, ³ J_{HH} = 6.2 Hz, 2H, C4-H), 5.66 (d, ³ J_{HH} = 6.2 Hz, 2H, C3-H), 4.31 (t, ³ J_{HH} = 11.4 Hz, 2H, C9-H), 2.83 (hept, ³ J_{HH} = 6.9 Hz, 1H, C6-H); 2.51, 2.37 (d, ³ J_{HH} = 12.0 Hz, 2H/2H, CH₂); 2.29 (s, 3H, C1-H); 2.01 (d, J = 13.3 Hz, 2H), 1.91 (d, J = 13.4 Hz, 2H), 1.81–1.69 (m, 4H), 1.58–1.38 (m, 4H) (CH₂); 1.22 (d + m, ³ J_{HH} = 6.6 Hz, 10H, C7-H + CH₂). ¹³C{¹H} NMR (CDCl₃): δ/ppm = 163.6 (C8), 109.2 (C5), 104.1 (C2), 87.2 (C4), 86.8 (C3), 76.1 (C9); 35.3, 33.3 (C10 + C10'); 31.7 (C6); 26.0, 25.6 (C11 + C11'); 25.4 (C12), 22.4 (C7), 19.0 (C1).

[RuCl(η⁶-*p*-cymene){κ²N-(HCN(4-C₆H₄CH₃))₂][CF₃SO₃], **4[CF₃SO₃](Chart 2)**

Chart 2. Structure of **4**[CF₃SO₃](numbering refers to carbon atoms).

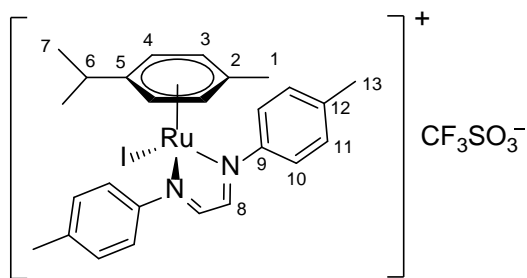


A suspension of $[\text{RuCl}_2(\eta^6\text{-}p\text{-cymene})]_2$ (142 mg, 0.232 mmol) in MeCN was treated with $\text{Ag}(\text{CF}_3\text{SO}_3)$ (120 mg, 0.467 mmol) and stirred at room temperature for 1 h under protection from the light. The resulting suspension (yellow solution + colorless AgCl precipitate) was filtered over a celite pad then N,N -bis(4-methylphenyl)ethylenediamine (110 mg, 0.464 mmol) was added to the filtrate. The orange suspension was heated at reflux for 4 h, affording a dark red solution. Next, volatiles were removed under vacuum; the residue was triturated in Et_2O :hexane 1:1 v/v and filtered. The resulting dark red-brown solid was washed with Et_2O :hexane 1:1 v/v and dried under vacuum (40 °C). Yield: 299 mg, 98 %. Compound $\mathbf{4}[\text{CF}_3\text{SO}_3]$ was also obtained by the reaction of $\mathbf{4}[\text{NO}_3]$ (82 mg, 0.14 mmol) with $\text{Ag}(\text{CF}_3\text{SO}_3)$ (37 mg, 0.15 mmol) in refluxing CHCl_3 (8 mL), as previously described for $\mathbf{2}[\text{CF}_3\text{SO}_3]$. Yield: 50 mg, 50 %. Compound $\mathbf{4}[\text{CF}_3\text{SO}_3]$ is soluble in MeOH, CH_2Cl_2 , CHCl_3 , MeCN, poorly soluble in Et_2O and insoluble in hexane. X-ray quality crystals of $\mathbf{4}[\text{CF}_3\text{SO}_3]$ were collected from a CH_2Cl_2 solution layered with Et_2O and settled aside at -20°C . Anal. Calcd. For $\text{C}_{27}\text{H}_{30}\text{ClF}_3\text{N}_2\text{O}_3\text{RuS}$: C, 49.43; H, 4.61; N, 4.27. Found: 48.75; H, 4.52; N, 4.17. IR (solid state): $\tilde{\nu}/\text{cm}^{-1} = 3063\text{w}, 2984\text{w}, 2965\text{w}, 2933\text{w}, 2911\text{w}, 2871\text{w}, 1605\text{w} (\nu_{\text{C}=\text{N}}), 1535\text{w}, 1501\text{m}, 1473\text{w}, 1461\text{w}, 1390\text{w}, 1388\text{w}, 1272\text{s-sh} (\nu_{\text{S}=\text{O}}), 1259\text{s} (\nu_{\text{S}=\text{O}}), 1223\text{m}, 1177\text{m-sh}, 1164\text{m-sh}, 1146\text{s}, 1115\text{w}, 1093\text{w}, 1068\text{w}, 1051\text{w}, 1029\text{s} (\nu_{\text{S}-\text{O}}), 966\text{w}, 955\text{w}, 888\text{w}, 843\text{w}, 817\text{s}, 771\text{w}, 754\text{w}, 711\text{w}$. Λ_{m} (MeOH, $c = 1.0 \cdot 10^{-3} \text{ M}$) = $136 \text{ S} \cdot \text{cm}^2 \cdot \text{mol}^{-1}$. $^1\text{H NMR}$ (CD_3OD): $\delta/\text{ppm} = 8.47 \text{ (s, 2H, C8-H)}, 7.69 \text{ (d, } ^3J_{\text{HH}} = 8.2 \text{ Hz, 4H, C10-H)}, 7.46 \text{ (d, } ^3J_{\text{HH}} = 8.1 \text{ Hz, 4H, C11-H)}, 5.48 \text{ (d, } ^3J_{\text{HH}} = 6.4 \text{ Hz, 2H, C4-H)}, 5.42 \text{ (d, } ^3J_{\text{HH}} = 6.4 \text{ Hz, 2H, C3-H)}, 2.50 \text{ (s, 6H, C13-H)}, 2.41 \text{ (m, 1H, C6-H)}, 2.28 \text{ (s, 3H, C1-H)}, 1.05 \text{ (d, } ^3J_{\text{HH}} = 6.9 \text{ Hz, 6H, C7-H)}$. $^1\text{H NMR}$ (CDCl_3): $\delta/\text{ppm} = 8.33 \text{ (s, 2H, C8-H)}, 7.79 \text{ (d, } ^3J_{\text{HH}} = 8.3 \text{ Hz, 4H, C10-H)}, 7.33 \text{ (d, } ^3J_{\text{HH}} = 8.1 \text{ Hz, 4H, C11-H)}, 5.24 \text{ (d, } ^3J_{\text{HH}} = 6.4 \text{ Hz, 2H, C4-H)}, 5.19 \text{ (d, } ^3J_{\text{HH}} = 6.4 \text{ Hz, 2H, C3-}$

H), 2.69 (hept, $^3J_{\text{HH}} = 7.0$ Hz, 1H, C6-H), 2.46 (s, 6H, C13-H), 2.13 (s, 3H, C1-H), 1.17 (d, $^3J_{\text{HH}} = 6.9$ Hz, 6H, C7-H). $^{13}\text{C}\{^1\text{H}\}$ NMR (CDCl_3): $\delta/\text{ppm} = 164.8$ (C8), 150.4 (C9), 141.4 (C12), 130.3 (C11), 124.2 ($^1J_{\text{CF}} = 310.4$ Hz, CF_3), 122.4 (C10), 110.4 (C5), 103.7 (C2), 88.2 (C3), 87.4 (C4), 30.9 (C6), 22.3 (C7), 21.5 (C13), 18.4 (C1). ^{19}F NMR (CDCl_3): $\delta/\text{ppm} = -78.2$ ppm.

$[\text{RuI}(\eta^6\text{-}p\text{-cymene})\{\kappa^2\text{N}(\text{HCN}(4\text{-C}_6\text{H}_4\text{CH}_3)_2)\}][\text{CF}_3\text{SO}_3]$, $6[\text{CF}_3\text{SO}_3]$ (Chart 3)

Chart 3. Structure of $6[\text{CF}_3\text{SO}_3]$ (numbering refers to carbon atoms).



A solution of KI (26 mg, 0.16 mmol) in MeOH (1 mL) was added dropwise to hot (*ca.* 50°C) solution of $4[\text{CF}_3\text{SO}_3]$ (96 mg, 0.15 mmol) in CHCl_3 (10 mL) under stirring. The mixture was heated for 3 h under protection from the light, then volatiles were removed under vacuum. The residue was suspended in CH_2Cl_2 and filtered over a celite pad. Volatiles were removed under vacuum from the filtrate solution and the resulting dark red-purple solid was washed with Et_2O and dried under vacuum (40 °C). Yield: 96 mg, 88 %. Alternatively, a solution of $4[\text{CF}_3\text{SO}_3]$ (28 mg, 0.042 mmol) and $[\text{Me}_4\text{N}]\text{I}$ (9.0 mg, 0.045 mmol) in CH_2Cl_2 (5 mL) was stirred at room temperature for 24 h. Next, the mixture was extracted with H_2O (3 x 10 mL) and the organic phase was dried under vacuum. Yield: 25 mg, 82 %. Compound $6[\text{CF}_3\text{SO}_3]$ is soluble in MeOH, CH_2Cl_2 , CHCl_3 ; insoluble in Et_2O and hexane. Anal. Calcd. for $\text{C}_{27}\text{H}_{30}\text{F}_3\text{IN}_2\text{O}_3\text{RuS}$: C, 43.38; H, 4.05; N, 3.75. Found: C, 43.2; H, 3.99; N, 3.70. IR (solid state): $\tilde{\nu}/\text{cm}^{-1} = 3063\text{w}$, 3040w , 2964w , 2924w , 2871w , 1602w ($\nu_{\text{C}=\text{N}}$), 1558w , 1540w , 1501m , 1470m , 1381w , 1366w-sh , 1272s-sh ($\nu_{\text{S}=\text{O}}$), 1257s ($\nu_{\text{S}=\text{O}}$), 1223s-sh , 1177m-sh , 1150s , 1112m-sh , 1088w , 1054w , 1029s ($\nu_{\text{S-O}}$), 1018m-sh , 961w , 877w , 864w , 816s , 773w , 754w , 710w . Λ_{m} (MeOH, $c = 1.0 \cdot 10^{-3}$ M) = $127 \text{ S} \cdot \text{cm}^2 \cdot \text{mol}^{-1}$. ^1H NMR (CD_3OD): $\delta/\text{ppm} = 8.43$ (s, 2H, C8-H), 7.78 (d, $^3J_{\text{HH}} = 8.3$ Hz, 4H,

C10-H), 7.43 (d, $^3J_{\text{HH}} = 8.1$ Hz, 4H, C11-H), 5.44 (s, 4H, C3-H + C4-H), 2.56 (s, 3H, C1-H), 2.50 (s, 6H, C13-H), 2.48–2.39 (m, 1H, C6-H), 1.03 (d, $^3J_{\text{HH}} = 6.9$ Hz, 6H, C7-H). ^{19}F NMR (CD_3OD): $\delta/\text{ppm} = -80.1$ ppm. ^1H NMR (CDCl_3): $\delta/\text{ppm} = 8.33$ (s, 2H, C8-H), 7.95 (d, $^3J_{\text{HH}} = 7.2$ Hz, 4H, C10-H), 7.30 (d, $^3J_{\text{HH}} = 7.9$ Hz, 4H, C11-H), 5.20 (s, 4H, C3-H + C4-H), 2.92 (hept, $^3J_{\text{HH}} = 6.8$ Hz, 1H, C6-H), 2.45 (s, 6H, C13-H), 2.22 (s, 3H, C1-H), 1.14 (d, $^3J_{\text{HH}} = 6.8$ Hz, 6H, C7-H). $^{13}\text{C}\{^1\text{H}\}$ NMR (CDCl_3): $\delta/\text{ppm} = 163.2$ (C8), 151.2 (C9), 141.1 (C12), 130.1 (C11), 123.1 (C10), 111.2 (C5), 103.5 (C2); 88.6, 86.7 (C3 + C4); 31.7 (C6), 22.5 (C7), 21.5 (C13), 19.8 (C1).

3. X-Ray crystallography.

Crystal data and collection details for **4**[CF_3SO_3] are reported in Table 6. Data were recorded on a Bruker APEX II diffractometer equipped with a PHOTON2 detector using Mo– $\text{K}\alpha$ radiation. Data were corrected for Lorentz polarization and absorption effects (empirical absorption correction SADABS).⁴⁸ The structures were solved by direct methods and refined by full-matrix least-squares based on all data using F^2 .⁴⁹ Hydrogen atoms were fixed at calculated positions and refined by a riding model. All non-hydrogen atoms were refined with anisotropic displacement parameters.

Table 6. Crystal data and measurement details for **4**[CF_3SO_3].

Formula	$\text{C}_{27}\text{H}_{30}\text{ClF}_3\text{N}_2\text{O}_3\text{RuS}$
FW	656.11
T, K	100(2)
λ , Å	0.71073
Crystal system	Orthorhombic
Space group	$Pbca$
a , Å	11.0016(10)
b , Å	16.7631(15)
c , Å	29.518(3)
Cell Volume, Å ³	5443.7(9)
Z	8
D_c , g·cm ⁻³	1.601

μ , mm ⁻¹	0.804
F(000)	2672
Crystal size, mm	0.16 x 0.13 x 0.12
θ limits, °	2.309 – 25.049
Reflections collected	51787
Independent reflections	4753 ($R_{int} = 0.0841$)
Data / restraints / parameters	4753 / 234 / 348
Goodness of fit on F^2	1.373
R_1 ($I > 2\sigma(I)$)	0.1475
wR_2 (all data)	0.3023
Largest diff. peak and hole, e Å ⁻³	1.701 and –4.237

4. Speciation and stability in aqueous media.

Solubility in water (D₂O). The selected Ru compound was suspended in a D₂O solution (0.8mL) containing dimethyl sulfone (Me₂SO₂; $c = 3.28 \cdot 10^{-3}$ M) and stirred at 21 °C for 3 h. The resulting saturated solution was filtered over celite, transferred into an NMR tube and analyzed by ¹H NMR spectroscopy (delay time = 3 s; number of scans = 20). The concentration (= solubility) was calculated by the relative integral with respect to Me₂SO₂ as internal standard⁵⁰ [$\delta/\text{ppm} = 3.14$ (s, 6H)] (Table 1).

Octanol-water partition coefficient (log P_{ow}). Partition coefficients (P_{ow} ; IUPAC: K_D partition constant⁵¹), defined as $P_{ow} = c_{org}/c_{aq}$, where c_{org} and c_{aq} are molar concentrations of the selected compound in the organic and aqueous phase, respectively, were determined by the shake-flask method and UV-Vis measurements.⁵² Deionized water and 1-octanol were vigorously stirred for 24 h, to allow saturation of both phases, then separated by centrifugation. A stock solution of the selected Ru compound (*ca.* 2 mg; **4**[NO₃], **5**[NO₃], **6**[CF₃SO₃]) was prepared by first adding acetone (50 μ L, to help solubilization), followed by water-saturated octanol (2.5 mL). The solution was diluted with water-saturated octanol (*ca.* 1:3 v/v ratio, $c_{Ru} \approx 10^{-4}$ M, so that $1.5 \leq A \leq 2.0$ at λ_{max}) and its UV-Vis spectrum was recorded (A^0_{org}). An aliquot of the solution ($V_{org} = 1.2$ mL) was transferred into a test tube and octanol-saturated water ($V_{org} = V_{aq} = 1.2$ mL) was added. The mixture was vigorously stirred for 15 min at 21 °C then centrifuged (5000 rpm, 5 min). The UV-Vis spectrum of the organic phase was

recorded ($A_{\text{org}}^{\text{f}}$) and the partition coefficient was calculated as $P_{\text{ow}} = A_{\text{org}}^{\text{f}} / (A_{\text{org}}^0 - A_{\text{org}}^{\text{f}})$ where A_{org}^0 and $A_{\text{org}}^{\text{f}}$ are the absorbance in the organic phase before and after partition with the aqueous phase, respectively.^{52c} The partition coefficient was calculated as $P_{\text{ow}} = (A_{\text{aq}}^0 - A_{\text{aq}}^{\text{f}}) / A_{\text{aq}}^{\text{f}}$ where A_{aq}^0 and A_{aq}^{f} are the absorbance in the aqueous phase before and after partition with the organic phase, respectively. The wavelength of the maximum absorption of each compound (360 - 420 nm range) was used for UV-Vis quantitation. An inverse procedure was adopted for **1**[PF₆], **2**[NO₃] and **3**[NO₃], starting from a stock aqueous solution. The procedure was repeated three times for each sample (from the same stock solution); results are given as mean \pm standard deviation (Table 1).

Stability and hydrolysis in D₂O or D₂O/CD₃OD mixtures. The selected Ru compound (*ca.* 4 mg) was dissolved with a D₂O solution containing Me₂SO₂ ($3.28 \cdot 10^{-3}$ M, 0.8 mL) or a CD₃OD/D₂O mixture (tot 0.80 mL), according to the water solubility. The orange-yellow (**1**⁺-**2**⁺) or dark red-brown (**3**⁺-**6**⁺) solution ($c_{\text{Ru}} \approx 7.8 \cdot 10^{-3}$ M) was stirred for 30 minutes then filtered over celite and analyzed by ¹H NMR (delay time = 3 s; number of scans = 20). Next, the solution was heated at 37 °C for 72 h and ¹H NMR analysis was repeated. The residual amount of starting material in solution (% with respect to the initial spectrum) was calculated by the relative integral with respect to Me₂SO₂ as internal standard⁵⁰ (Table 2). Subsequently, the AgNO₃ (0.11 M in D₂O, 50 μ L, 1.0 eq) was added to each solution: no change was observed (*i.e.* AgCl opalescence or precipitate). The solution was heated at 50 °C in the dark for 3 h, then filtered over celite and analyzed by ¹H NMR. Finally, the solution was kept at 50 °C for additional 24 h, and the above procedure was repeated. The % hydrolyzed compound was calculated as a molar ratio with respect to the starting material (Table 2). ¹H NMR spectra and data for the tested compounds are reported in the Supporting Information (Figures S10-S15); ¹H NMR signals are referenced to Me₂SO₂ peak as in pure D₂O [$\delta/\text{ppm} = 3.14$ (s, 6H)].

Stability in cell culture medium. Powdered Dulbecco's Modified Eagle Medium (DMEM; 1000 mg/L glucose and L-glutamine, without sodium bicarbonate and phenol red; D2902 - Sigma Aldrich) was dissolved in D₂O (10 mg/mL), according to the manufacturer's instructions. The solution of

deuterated cell culture medium (“DMEM-d”) was treated with Me_2SO_2 ($6.6 \cdot 10^{-3}$ M) and NaH_2PO_4 / Na_2HPO_4 (0.15 M, $\text{pD} = 7.5^{53}$), then stored at 4 °C under N_2 . The selected Ru compound (3-4 mg) was dissolved in DMEM-d or in a DMEM-d/ CD_3OD solution (0.80 mL total volume), according to the water solubility. The orange-yellow ($\mathbf{1^+-2^+}$), dark green ($\mathbf{3^+}$) or dark red-brown ($\mathbf{4^+-6^+}$) solution ($c_{\text{Ru}} \approx 7.7 \cdot 10^{-3}$ M) was stirred for 30 minutes then filtered over celite and analyzed by ^1H NMR (delay time = 3 s; number of scans = 20). The solution was heated at 37 °C for 24 h, then ^1H NMR analysis was repeated. In each case, no new $\{\text{Ru}(\eta^6\text{-}p\text{-cymene})\}$ species was identified. The residual amount of starting material in solution (% with respect to the initial spectrum) was calculated by the relative integral with respect to Me_2SO_2 as internal standard⁵⁰ (Table 2).

UV-spectra in H_2O ; pK_a determination for $\mathbf{3}[\text{NO}_3]$. Spectrophotometric measurements were conducted on a double beam Shimadzu 2450 apparatus or a Hewlett-Packard 8453A (Agilent Technologies, Palo Alto, CA) photodiode array spectrophotometer (both temperature-controlled to within ± 0.1 °C). Data treatment was conducted by means of OriginLab and HypSpecsoftwares. In the determination of the pK_a of $\mathbf{3^+}$, a solution of the metal complex (3.89×10^{-4} M) in water was left to stabilize overnight and then the pH of the solution was lowered to 2.0. Small amounts of NaOH or HClO_4 were used to vary the pH solution.

5. Biological studies.

Materials Bovine serum albumin (BSA) was supplied by Sigma-Aldrich as crystallized and lyophilized powder ($\geq 98\%$, agarose gel electrophoresis and $\leq 0.005\%$ fatty acids); its concentration was spectrophotometrically determined ($\epsilon_{278 \text{ nm}} = 45000 \text{ M}^{-1} \text{ cm}^{-1}$).⁵⁴ Calf thymus DNA (lyophilized sodium salt, highly polymerized) from Sigma-Aldrich was dissolved in water and sonicated, producing short polynucleotide fragments (ca. 300 base pairs). The molar DNA concentration was spectrophotometrically determined ($\epsilon_{260 \text{ nm}} = 13200 \text{ M}^{-1} \text{ cm}^{-1}$) and is expressed in base pairs.⁵⁵ Plasmid pUC18 (2686 bp) was extracted from *Escherichia coli* DH5 α and purified by a HP Plasmid Midi kit

(Omega Biotek, VWR). The solutions of ethidium bromide solution (EtBr, purity > 99%, Sigma) were obtained by dissolving the appropriate amount of the solid in the buffer; their molar concentration was evaluated spectrophotometrically ($\epsilon_{480\text{ nm}} = 5600\text{ M}^{-1}\text{ cm}^{-1}$).⁵⁶ Chemicals not expressly cited are of analytical grade and were used without further purification. Appropriate amounts of **1**[PF₆], **2-5**[NO₃], **6**[CF₃SO₃] were accurately weighted and dissolved in dimethyl sulfoxide (DMSO) to get ca. 10⁻³-10⁻² M stock solutions. Solutions of BSA, DNA and EtBr in buffer, were freshly prepared and kept at 4 °C in the dark. The buffer is an aqueous solution of 0.1 M NaCl and 2.5 mM NaCac (sodium cacodylate) for BSA, and aqueous solution 2.5 mM NaCac for DNA. The water used to prepare the solutions and as a reaction medium was ultrapure 18.2 MΩ water from a Sartorius purification system. Measurements of pH were made by a Metrohm 713 pH- metre equipped with a combined glass electrode.

Cytotoxic activity. A549 (lung adenocarcinoma) cells were cultured Dulbecco's Modified Eagle's Medium (DMEM), A2780 (ovarian carcinoma) were cultured in RPMI 1640 medium supplemented with 2 mM L-glutamine and HEK293 (embryonic kidney) cells were cultured in Eagle's Minimum Essential Medium (EMEM) supplemented with 1% of non-essential amino acids. All culture media were supplemented with 10% fetal bovine serum (FBS) and 1% amphotericin-penicillin-streptomycin solution. To conduct cytotoxicity tests, approximately 3 × 10³ A549 and A2780 and 1 × 10⁴ HEK293 cells were cultured in 200 μL culture medium per well in 96-well plates and incubated in a humid atmosphere at 37°C under 5% CO₂ atmosphere for 24h. Cells were then incubated for 72 h with 100 μL of culture medium with different concentrations of the metal complexes (0, 1.25, 5, 12.5, 25 and 50 μM) in culture medium. Cisplatin (**cPt**) was also included as the control. Metal complexes were first dissolved in DMSO whereas cisplatin was dissolved in water, then they were diluted in the culture medium. The DMSO concentration was kept under 0.5% DMSO. A control experiment containing the same amount of DMSO was included. Then, after removing the medium, 100 μL of 500 μg mL⁻¹ of MTT (thiazolyl blue tetrazolium bromide) was added to each well and incubated for 4 h. Lastly, the formazan product was dissolved by adding 100 μL of solubilizing solution (10% sodium dodecyl

sulfate (SDS) in 0.01 M HCl) and allowing the solution to solubilize overnight. Absorbance was read at 590 nm in a microplate reader (Biotek Instruments). Four replicates per dose were included in each experiment, and half-maximal inhibitory concentration (IC₅₀) values were calculated using the GraphPad Prism 6.01 analysis software (GraphPad Software Inc.) from three independent experiments.

Bioimaging experiments. A549 cells were grown for 24 h and then exposed to 5, 10, 30 and 50 μ M of the compounds during 24 h. Then, cells were visualized in a Cytation 5 Cell Imaging Multi-Mode Reader (Biotek Instruments, USA) in bright field with a 20 \times objective.

Ruthenium cellular uptake. A549 cells were seeded in 6-well plates ($1.5 \cdot 10^5$ cells/well) and grown for 24h at 37°C and 5% CO₂. Subsequently, cells were exposed to 2 μ M solution of the drug for 24h, washed for three times with DPBS (Dulbecco's Phosphate Buffered Saline), trypsinized and centrifugated. The pellets were resuspended in 1 mL of DPBS and in each case, 10 μ L were used to count cells in an automated cell counter (BioRad). The samples were digested with 65% HNO₃ at room temperature during 24h. Lastly, solutions were analyzed in an 8900 ICP-MS (Agilent Technologies). Data are reported as the mean of three independent experiments.

Antimicrobial activity. Antimicrobial activity was studied by means of the broth microdilution plate method according to CLSI criteria against ESKAPE pathogens.⁵⁷ *E. faecium* CECT 5253 (vancomycin resistant, Gram positive bacteria), *S. aureus* CECT 5190 (methicillin resistant, Gram positive bacteria), *A. baumannii* ATCC 17978 (Gram negative bacteria) and *P. aeruginosa* PAOI (Gram negative bacteria) were included. Minimum Inhibitory concentration (MIC) was defined as the lowest concentration of the tested compound that inhibited bacterial growth. The MICs reported are the mean values of three replicates. At least two independent experiments were performed.

Electrophoresis and circular dichroism. Native polyacrylamide gel electrophoresis (PAGE) of BSA were done after overnight incubation at 37 °C of the protein (1 μ M) in the presence of different concentrations of complexes ($C_D/C_{BSA} = 10$ and 30). After that, 5 μ L of sample buffer 2 \times (0.01% bromophenol blue and 20% glycerol in TrisHCl buffer (0.5 M, pH 6.8) were added to 5 μ L of the

sample solutions and loaded onto 10% polyacrylamide gels. Gels were run in native PAGE buffer (250 mM Tris Base, 1.92 M glycine, pH = 8.3) at 6.6 V/cm for 6 h at 4°C to avoid thermal denaturation of the protein. Finally, gels were stained with Coomassie brilliant blue R-250 and visualized with a Gel Doc XR+ Imaging System (Bio Rad).

Circular Dichroism (CD) experiments were performed with a MOS-450 biological spectrophotometer (Bio-Logic SAS, Claix, France). BSA in the absence and in the presence of the Ru(II) complexes under study were prepared in 2.5 mM sodium cacodylate (NaCaC) buffer at pH = 7.0 and T = 25 °C.

Agarose gel electrophoresis of plasmid DNA (pUC18) was performed after overnight incubation at 37.0 °C of the plasmid (3.7 µM, base pairs) in the presence of different concentrations of complexes ($C_D/C_{DNA} = 0.5, 1.5, 3.0, 5.0$ for **1**, **2**, **5** and **7**; $C_D/C_{DNA} = 0.5, 1.0, 1.5, 2.0, 3.0, 4.0$ and 5.0 for **3** and **4**) or cisplatin ($C_D/C_{DNA} = 0.5, 1.0, 1.5, 2.0, 3.0, 4.0, 5.0$) in buffer (NaCac 2.5 mM, pH 7.0). Samples were loaded onto 1% agarose gel and electrophoresis was run at 6.5V/cm during 150 min. After the run, the gel was stained with a solution of ethidium bromide 1 µg/mL in TBE 1× for 30 minutes. Finally, the gel was visualized by exposure to UV light (312 nm) by a Gel Doc XR+ Imaging System (Bio-Rad).

DNA and BSA spectrophotometric titrations. Spectrophotometric titrations were done on the already described UV-vis instruments; light emission measurements were done using a Perkin Elmer LS55 instrument. The actual temperature inside the cell compartment was controlled by a mini-thermometer. Any addition during spectroscopic titrations was done directly into the cell by means of a glass syringe connected to a micrometric screw (Mitutoyo, one complete turn of the screw equal to 8.2 µL). For both EtBr displacement and BSA titration, blank tests were carried out by adding DMSO to the sample cell, in order to quantify fluorescence changes due to dilution/solvent effects. Since solvent effects were observed, to reduce the maximum amount of DMSO to 0.1 %, highly concentrated stock solutions were prepared (of the order of 10^{-2} M), which were diluted in buffer to 10^{-4} M. This was not possible for **5**⁺ and **6**⁺ due to their low solubility in water. Ethidium Bromide displacement assays were done in a

diluted buffered solution of NaCac 2.5 mM at pH 7.0 (no NaCl). This was needed due to the high extinction molar coefficients of some compounds which required to work with diluted solutions for both metal complex and DNA. Under these circumstances, saturation of DNA with the EtBr dye is not achieved if the process is not favored by lowering salt content. To avoid inner filter effects which could bias our results, the titrations were stopped as the maximum absorption at the excitation (A_{ex}^{λ}) and emission (A_{em}^{λ}) wavelengths of the system reached 0.1. Also, the equation $F_{\text{corr}} = F_{\text{obs}} \times 10^{(A_{\text{ex}}^{\lambda} + A_{\text{em}}^{\lambda})/2}$ was used to correct the observed fluorescence values F_{obs} at any point of the titration for the inner filter effect.³³ For the complex/BSA fluorescence titrations, a solution the metal complexes ($C_D \approx 1 \times 10^{-4}$ M in buffer NaCl 0.1 M, NaCac 2.5 mM, pH 7.0, DMSO 1 %) was added to BSA solution ($C_{\text{BSA}} \approx 1.5 \times 10^{-6}$ M $\lambda_{\text{ex}} = 280$ nm, $\lambda_{\text{em}} = 350$ nm). During the spectrophotometric titrations, appropriate amounts of the titrant (DNA) were directly added to the sample cell. In EtBr/DNA exchange experiments, DNA was saturated with EtBr ($\lambda_{\text{ex}} = 520$ nm, $\lambda_{\text{em}} = 595$ nm). Subsequently, increasing amounts of the complex stock solution were added to the EtBr/DNA mixture.

As for data processing and calculations, the equilibrium constant for the binding process to BSA (K) was determined by equation (1)

$$\frac{C_{\text{BSA}}}{\Delta F} = \frac{1}{K \cdot \Delta \varphi} \cdot \frac{1}{[i]} + \frac{1}{\Delta \varphi} \quad (1)$$

Here, C_{BSA} is the total molar concentration of BSA, $[i]$ is the molar concentration of the free tested ruthenium complex and $\Delta \varphi = \varphi_{\text{boundBSA}} - \varphi_{\text{unboundBSA}}$ is the change in the optical parameters, being under these diluted conditions $F_i = \varphi_i[i]$; note that the exact calculation of $[i]$ requires an iterative procedure [REF 33]. The non-quantitative binding between DNA and 6^+ was calculated by the combined use of equations (2) and (3) [REF 35]

$$\frac{C_P(C_D \Delta \varepsilon - \Delta A)}{\Delta A} = \frac{1}{nK} + \frac{(C_D \Delta \varepsilon - \Delta A)}{\Delta \varepsilon} \frac{1}{n} \quad (2)$$

$$\frac{C_D}{\Delta F} = \frac{1}{K \cdot \Delta \varphi} \cdot \frac{1}{C_P f(r)} + \frac{1}{\Delta \varphi} \quad (3)$$

where $C_P = C_{\text{DNA}}$, $C_D = C_{\text{complex}}$, K is the binding constant, $f(r) = (1-nr)^n/[1-(n-1)r]^{n-1}$, $r = \Delta F/(\Delta\phi C_P)$ and n corresponds to the site size.

Viscosity measurements were performed using a Cannon-Ubbelohde capillary viscometer (Schott) immersed in a water bath at 25.0 °C. The flow time was measured with a digital stopwatch. The sample viscosity was evaluated as the mean value of at least four replicated measurements. The viscosity readings were reported as $L/L_0 = (\eta/\eta_0)^{1/3}$ versus C_D/C_{DNA} ratio, where η and η_0 stand for the polynucleotide viscosity in the presence and in the absence of the metal complex, respectively. Here, $\eta = t - t_0$ whereas $\eta_0 = t_r - t_0$ and t is the flow time the sample solution, t_0 is the flow time of the solvent alone and t_r is the time of the reference (DNA alone).

Conflicts of interest

There are no conflicts to declare.

Acknowledgements

The University of Pisa (PRA_2020_39), “la Caixa” Foundation (LCF/PR/PR12/11070003), Ministerio de CienciaInnovación y Universidades-FEDER (RTI2018-102040-B-100) and Junta de Castilla y León-FEDER (BU305P18) are gratefully acknowledged for financial support. This contribution is also based upon work from COST Action CA18202, NECTAR - Network for Equilibria and Chemical Thermodynamics Advanced Research, supported by COST (European Cooperation in Science and Technology).

Supporting Information Available

NMR and IR spectra of new compounds. Stability and hydrolysis studies in aqueous media (^1H NMR spectra and NMR). UV-Vis characterization of compounds; pK_a determination for $\mathbf{3}^+$. Microscopy images of A149 cells. Interaction with BSA and DNA via

spectrophotometric/spectrofluorimetric titrations (UV-Vis spectra and thermodynamic data). CCDC reference number 2058423 (**4**[CF₃SO₃]) contains the supplementary crystallographic data for the X-ray study reported in this paper. These data can be obtained free of charge at <https://www.ccdc.cam.ac.uk/structures/> (or from the Cambridge Crystallographic Data Centre, 12, Union Road, Cambridge CB2 1EZ, UK; fax: (internat.) +44-1223/336-033; e-mail: deposit@ccdc.cam.ac.uk).

Notes and Reference

- ¹ NAMI-A = (ImidazoleH)[*trans*-RuCl₄(κS-DMSO)(κN-Imidazole)]; KP1019 = (IndazoleH)[*trans*-RuCl₄(κN-Indazole)₂]; (N)KP1339/IT-139 = Na[*trans*-RuCl₄(κN-Indazole)₂]; TLD1433 = (4,4'-dimethyl-2,2'-bipyridine)(α-terthienylimidazo[4,5-f][1,10]-phenanthroline)ruthenium(II) dichloride.
- ² (a) S. Leijen, S. A. Burgers, P. Baas, D. Pluim, M. Tibben, E. van Werkhoven, E. Alessio, G. Sava, J. H. Beijnen, J. H. M. Schellens, Phase I/II study with ruthenium compound NAMI-A and gemcitabine in patients with non-small cell lung cancer after first line therapy, *Invest. New Drugs* 33 (2015) 201–214. (b) H. A. Burris, S. Bakewell, J. C. Bendell, J. Infante, S. F. Jones, D. R. Spigel, G. J. Weiss, R. K. Ramanathan, A. Ogden, D. Von Hoff, Safety and activity of IT-139, ruthenium-based compound, in patients with advanced solid tumours: a first-in-human, open-label, dose-escalation phase I study with expansion cohort, *ESMO Open* 1 (2016) e000154. (c) S. Monro, K. L. Colon, H. Yin, J. Roque, P. Konda, S. Gujar, R. P. Thummel, L. Lilge, C. G. Cameron, S. A. McFarland, Transition Metal Complexes and Photodynamic Therapy from a Tumor-Centered Approach: Challenges, Opportunities, and Highlights from the Development of TLD1433, *Chem. Rev.* 119 (2019) 797–828. (d) E. Alessio, L. Messori, NAMI-A and KP1019/1339, Two Iconic Ruthenium Anticancer Drug Candidates Face-to-Face: A Case Story in Medicinal Inorganic Chemistry, *Molecules* 2019, 24, 1995; doi:10.3390/molecules24101995.
- ³ (a) E. J. Anthony, E. M. Bolitho, H. E. Bridgewater, O. W. L. Carter, J. M. Donnelly, C. Imberti, E. C. Lant, F. Lermyte, R. J. Needham, M. Palau, P. J. Sadler, H. Shi, F.-X. Wang, W.-Y. Zhang, Z. Zhang, Metallodrugs are unique: opportunities and challenges of discovery and development, *Chem. Sci.*, 2020, 11, 12888–12917. (b) B. S. Murray, P. J. Dyson, Recent progress in the development of organometallics for the treatment of cancer, *Curr. Opin. Chem. Biol.* 2020, 56, 28–34. (c) Nazarov, A. A.; Hartinger, C. G.; Dyson, P. J. Opening the Lid on Piano-Stool Complexes: An Account of Ruthenium(II)–Arene Complexes with Medicinal Applications. *J. Organomet. Chem.* 751 (2014) 251–260.
- ⁴ (a) M. Rausch, P. J. Dyson, P. Nowak-Sliwinska, Recent Considerations in the Application of RAPTA-C for Cancer Treatment and Perspectives for Its Combination with Immunotherapies, *Adv. Therap.* 2 (2019) 1900042. (b) B. S. Murray, M. V. Babak, C. G. Hartinger, P. J. Dyson, The development of RAPTA compounds for the treatment of tumors, *Coord. Chem. Rev.* 2016, 306, 86–114.
- ⁵ S. M. Meier-Menches, C. Gerner, W. Berger, C. G. Hartinger, B. K. Keppler, Structure–activity relationships for ruthenium and osmium anticancer agents – towards clinical development, *Chem. Soc. Rev.* 47 (2018) 909–928.
- ⁶ A. F. A. Peacock, P. J. Sadler, Medicinal Organometallic Chemistry: Designing Metal Arene Complexes as Anticancer Agents, *Chem. Asian J.* 3 (2008) 1890–1899.

- ⁷ (a) L. Biancalana, K. K. Batchelor, T. Funaioli, S. Zacchini, M. Bortoluzzi, G. Pampaloni, P. J. Dyson, F. Marchetti, α -Diimines as Versatile, Derivatizable Ligands in Ruthenium(II) p-Cymene Anticancer Complexes. *Inorg. Chem.* 57 (2018), 6669–6685. (b) L. Biancalana, S. Fulignati, C. Antonetti, S. Zacchini, G. Provinciali, G. Pampaloni, A. M. Raspolli Galletti, F. Marchetti, *New J. Chem.* 42 (2018), 17574-17586.
- ⁸ M. Santi, A. K. Mapana, L. Biancalana, F. Marchetti, V. Voliani, Ruthenium arene complexes in the treatment of 3D models of head and neck squamous cell carcinomas, *Eur. J. Med. Chem.* 212 (2021) 113143.
- ⁹ (a) F. Wang, A. Habtemariam, E. P. L. van der Geer, R. Fernández, M. Melchart, R. J. Deeth, R. Aird, S. Guichard, F. P. A. Fabbiani, P. Lozano-Casal, I. D. H. Oswald, D. I. Jodrell, S. Parsons, P. J. Sadler, Controlling ligand substitution reactions of organometallic complexes: Tuning cancer cell cytotoxicity, *Proc. Natl. Acad. Sci. USA* 102 (2005) 18269-18274. (b) C. Scolaro, A. Bergamo, L. Brescacin, . Delfino, M. Cocchietto, G. Laurenczy, T. J. Geldbach, G. Sava, P. J. Dyson, In Vitro and in Vivo Evaluation of Ruthenium(II) – Arene PTA Complexes. *J. Med. Chem.* 2005, 48, 4161-4171.
- ¹⁰ (a) L. Zeng, P. Gupta, Y. Chen, E. Wang, L. Ji, H. Chao, Z.-S. Chen, The development of anticancer ruthenium(II) complexes: from single molecule compounds to nanomaterials, *Chem. Soc. Rev.* 46 (2017), 5771-5804. (b) O. Dömötör, É. A. Enyedy, Binding Mechanisms of Half-Sandwich Rh(III) and Ru(II) Arene Complexes on Human Serum Albumin: A Comparative Study. *J. Biol. Inorg. Chem.* 24 (2019), 703–719. (c) A. Merlino, T. Marzo, L. Messori, Protein Metalation by Anticancer Metallodrugs: A Joint ESI MS and XRD Investigative Strategy, *Chem. Eur. J.* 2017, 23, 6942 – 6947.
- ¹¹ T. Peters Jr. All About Albumin: Biochemistry, Genetics, and Medical Applications; Academic Press, 1995.
- ¹² W. Bal, J. Christodoulou, P. J. Sadler, A. Tucker, Multi-Metal Binding Site of Serum Albumin. *J. Inorg. Biochem.* 70 (1998), 33–39.
- ¹³ (a) N. M. Urquiza, L. G. Naso, S. G. Manca, L. Lezama, T. Rojo, P. A. M. Williams, E. G. Ferrer, Antioxidant Activity of Methimazole–Copper(II) Bioactive Species and Spectroscopic Investigations on the Mechanism of Its Interaction with Bovine Serum Albumin. *Polyhedron* 31 (2012), 530–538. (b) U. Kragh-Hansen, Molecular Aspects of Ligand Binding to Serum Albumin. *Pharmacol. Rev.* 33 (1981) 17–53.
- ¹⁴ R. L. Gurung, H. K. Lim, S. Venkatesan, P. S. W. Lee, M. P. Hande, Targeting DNA-PKcs and Telomerase in Brain Tumour Cells. *Mol. Cancer* 13 (2014) 232.
- ¹⁵ (a) N. Busto, J. Valladolid, M. Martínez-Alonso, H. J. Lozano, F. A. Jalón, B. R. Manzano, A. M. Rodríguez, M. Carmen Carrión, T. Biver, J. M. Leal, G. Espino, B. García, Anticancer Activity and DNA Binding of a Bifunctional Ru(II) Arene Aqua-Complex with the 2,4-Diamino-6-(2-pyridyl)-

- 1,3,5-triazine Ligand, *Inorg. Chem.* 52 (2013), 9962–9974. (b) M. Martínez-Alonso, N. Busto, F. A. Jalón, B. R. Manzano, J. M. Leal, A. M. Rodríguez, B. García, G. Espino, Derivation of Structure–Activity Relationships from the Anticancer Properties of Ruthenium(II) Arene Complexes with 2-Aryldiazole Ligands, *Inorg. Chem.* 53 (2014) 11274–11288
- ¹⁶ (a) F. Wang, H. Chen, S. Parsons, I. D. H. Oswald, J. E. Davidson, P. J. Sadler, Kinetics of Aquation and Anation of Ruthenium(II) Arene Anticancer Complexes, Acidity and X-Ray Structures of Aqua Adducts. *Chem. Eur. J.* 9 (2003), 5810–5820. (b) Z. Adhireksan, G. E. Davey, P. Campomanes, M. Groessl, C. M. Clavel, H. Yu, A. A. Nazarov, C. H. Fang Yeo, W. Han Ang, P. Droge, U. Rothlisberger, P. J. Dyson, C. A. Davey, Ligand substitutions between ruthenium–cymene compounds can control protein versus DNA targeting and anticancer activity, *Nat. Commun.* 5 (2014) 3462.
- ¹⁷ (a) O. Novakova, H. Chen, O. Vrana, A. Rodger, P. J. Sadler, V. Brabec, DNA Interactions of Monofunctional Organometallic Ruthenium(II) Antitumor Complexes in Cell-Free Media. *Biochemistry* 42 (2003), 11544–11554. (b) H. Chen, J. A. Parkinson, R. E. Morris, P. J. Sadler, Highly Selective Binding of Organometallic Ruthenium Ethylenediamine Complexes to Nucleic Acids: Novel Recognition Mechanisms. *J. Am. Chem. Soc.* 125 (2003), 173–186.
- ¹⁸ E. Carrillo, S. Ramírez-Rivera, G. Bernal, G. Aquea, C. Tessini, F. A. Thomet, *Life Sciences* 2019, 217, 193–201.
- ¹⁹ (a) S. Thangavel, M. Paulpandi, H. B. Friedrich, K. Sukesh, A. A. Skelton, New Ru(II) half sandwich complexes bearing the N,Nbidentate 9-ethyl-N-(pyridin-2-ylmethylene)9H-carbazole-3-amine ligand: Effects of halogen (Cl, Br and I) leaving groups versus in vitro activity on HepG2 cancer cells, cell cycle, fluorescence study, cellular accumulation and DFT study, *Polyhedron* 2018, 152, 37–48. (b) J. M. Gichumbi, B. Omondi, G. Lazarus, M. Singh, N. Shaikh, H. Y. Chenia, H. B. Friedrich, Influence of Halogen Substitution in the Ligand Sphere on the Antitumor and Antibacterial Activity of Half-sandwich Ruthenium(II) Complexes $[\text{RuX}(\eta^6\text{-arene})(\text{C}_5\text{H}_4\text{N}_2\text{-CH=N-Ar})]^+$, *Z. Anorg. Allg. Chem.* 2017, 643, 699–711. (c) A. M. Basri, R. M. Lord, S. J. Allison, A. Rodriguez-Barzano, S. J. Lucas, F. D. Janeway, H. J. Shepherd, C. M. Pask, R. M. Phillips, P. C. McGowan, Bis-picolinamide Ruthenium(III) Dihalide Complexes: Dichloride-to-Diodide Exchange Generates Single trans Isomers with High Potency and Cancer Cell Selectivity, *Chem. Eur. J.* 2017, 23, 6341–6356.
- ²⁰ (a) I. Romero-Canelón, L. Salassa, P. J. Sadler, The Contrasting Activity of Iodido versus Chlorido Ruthenium and Osmium Arene Azo- and Imino-pyridine Anticancer Complexes: Control of Cell Selectivity, Cross-Resistance, p53 Dependence, and Apoptosis Pathway. *J. Med. Chem.* 2013, 56, 1291–1300. (b) S. Moon, M. Hanif, M. Kubanik, H. Holtkamp, T. Schnell, S. M. F. Jamieson, C. G. Hartinger, Organoruthenium and Osmium Anticancer Complexes Bearing a Maleimide Functional Group: Reactivity to Cysteine, Stability, and Cytotoxicity, *ChemPlusChem* 2015, 80, 231–236. (c) S.

- Betanzos-Lara, O. Novakova, R. J. Deeth, A. M. Pizarro, G. J. Clarkson, B. Liskova, V. Brabec, P. J. Sadler, A. Habtemariam, Bipyrimidine ruthenium(II) arene complexes: structure, reactivity and cytotoxicity, *J BiolInorgChem* 2012, 17, 1033–1051. (d) S. J. Dougan, A. Habtemariam, S. E. McHale, S. Parsons, P. J. Sadler, Catalytic organometallic anticancer complexes, *PNAS* 2008, 105, 11628–11633. (e) A. Mukherjee, S. Acharya, K. Purkait, K. Chakraborty, A. Bhattacharjee, A. Mukherjee, Effect of N,N Coordination and Ru^{II} Halide Bond in Enhancing Selective Toxicity of a Tyramine-Based Ru^{II} (p-Cymene) Complex, *Inorg. Chem.* 59 (2020) 6581–6594.
- ²¹ F. Li, J. G. Collins, F. R. Keene, Ruthenium complexes as antimicrobial agents, *Chem. Soc. Rev.* 44 (2015) 2529–2542.
- ²² (a) J. Kljun, I. E. León, Š. Peršič, J. F. Cadavid-Vargas, S. B. Etcheverry, W. He, Y. Bai, I. Turel, Synthesis and biological characterization of organoruthenium complexes with 8-hydroxyquinolines, *J. Inorg. Biochem.* 186 (2018) 187–196. (b) Z. Ude, I. Romero-Canelón, B. Twamley, D. Fitzgerald Hughes, P. J. Sadler, C. J. Marmion, A novel dual-functioning ruthenium(II)–arene complex of an anti-microbial ciprofloxacin derivative — Anti-proliferative and anti-microbial activity, *J. Inorg. Biochem.* 160 (2016) 210–217.
- ²³ (a) M. Göttlicher, S. Minucci, P. Zhu, O. H. Krämer, A. Schimpf, S. Giavara, J. P. Sleeman, F. Lo Coco, C. Nervi, P. G. Pelicci, T. Heinzel, Valproic acid defines a novel class of HDAC inhibitors inducing differentiation of transformed cells. *The EMBO Journal* 20 (2001) 6969–6978. (b) L. Činčárová, Z. Zdráhal, J. Fajkus, New perspectives of valproic acid in clinical practice, *Expert Opin. Investig. Drugs*, 22 (2013) 1535–1547. (c) M. A. Głozak, E. Seto, *Oncogene* 26 (2007) 5420–5432.
- ²⁴ (a) P. Štarha, Z. Trávníček, R. Herchel, P. Jewula, Z. Dvořák, A potential method to improve the in vitro cytotoxicity of half-sandwich Os(II) complexes against A2780 cells, *Dalton Trans.* 47 (2018) 5714–5724. (b) V. Novohradsky, L. Zerzankova, J. Stepankova, O. Vrana, R. Raveendran, D. Gibson, J. Kasparkova, V. Brabec, Antitumor platinum(IV) derivatives of oxaliplatin with axial valproate ligands, *J. Inorg. Biochem.* 140 (2014) 72–79.
- ²⁵ P. Poolchanuan, P. Unagul, S. Thongnest, S. Wiyakrutta, N. Ngamrojanavanich, C. Mahidol, S. Ruchirawat, P. Kittakoo, An anticonvulsive drug, valproic acid (valproate), has effects on the biosynthesis of fatty acids and polyketides in microorganisms. *Sci. Rep.* 10(2020)9300.
- ²⁶ M. Rao, D. Valentini, A. Zumla, M. Maeurer, Evaluation of the efficacy of valproic acid and suberoylanilidehydroxamic acid (vorinostat) in enhancing the effects of first-line tuberculosis drugs against intracellular *Mycobacterium tuberculosis*, *Int. J. Infect. Dis.* 69 (2018) 78–84.
- ²⁷ I. Bratsos, T. Gianferrara, E. Alessio, C. G. Hartinger, M. A. Jakupec, B. K. Keppler, *Bioinorganic Medicinal Chemistry* (Ed.: E. Alessio), Wiley-VCH, Weinheim, 2011, pp. 151–174.
- ²⁸ T. Biver, F. Secco, M. R. Tinè, M. Venturini, Kinetics and equilibria for the formation of a new DNA metal-intercalator: the cyclic polyamine Neotrien/copper(II) complex, *J. Inorg. Biochem.* 2004, 98, 33–40.

- ²⁹ C. Pérez-Arnaiz, J. Leal, N. Busto, M. C. Carrión, A. R. Rubio, I. Ortiz, G. Barone, B. Díaz de Greñu, J. Santolaya, J. M. Leal, M. Vaquero, F. A. Jalón, B. R. Manzano, B. García, Role of Seroalbumin in the Cytotoxicity of cis-Dichloro Pt(II) Complexes with (N^N)-Donor Ligands Bearing Functionalized Tails, *Inorg. Chem.* 57 (2018) 6124–6134.
- ³⁰ Liu, F.; Gao, S.; Yang, Y.; Zhao, X.; Fan, Y.; Ma, W.; Yang, D.; Yang, A.; Yu, Y. Curcumin Induced Autophagy Anticancer Effects on Human Lung Adenocarcinoma Cell Line A549; Spandidos Publications 14 (2017), 2775–2782.
- ³¹ (a) A. M. Walker; J. J. Stevens, K. Ndebele, P. B. Tchounwou, Evaluation of Arsenic Trioxide Potential for Lung Cancer Treatment: Assessment of Apoptotic Mechanisms and Oxidative Damage. *J. Cancer Sci. Ther.* 8 (2016), 1-9. (b) I. Mendieta, R. E. Nuñez-Anita, G. Pérez-Sánchez, L. Pavón, A. Rodríguez-Cruz, G. García-Alcocer, L. C. Berumen, Effect of A549 Neuroendocrine Differentiation on Cytotoxic Immune Response. *Endocr. Connect.* 7 (2018), 791–802.
- ³² (a) F. Marchetti, C. Di Nicola, R. Pettinari, C. Pettinari, I. Aiello, M. La Deda, A. Candrea, S. Morelli, L. De Bartolo, A. Crispini, *Eur. J. Inorg. Chem.* 2020, 1027–1039. (b) V. R. Akhmetova, N. S. Akhmadiev, M. F. Abdullin, L. U. Dzhemileva, V. A. Dyakonov, Synthesis of new N,N-Pd(Pt) complexes based on sulfanylpurazoles, and investigation of their in vitro anticancer activity, *RSC Adv.* 2020, 10, 15116–15123.
- ³³ F. Macii, T. Biver, Spectrofluorimetric analysis of the binding of a target molecule to serum albumin: tricky aspects and tips, *J. Inorg. Biochem.* (2020), DOI: 10.1016/j.jinorgbio.2020.111305
- ³⁴ (a) S. Huang, S. Peng, W. Su, Z. Tang, J. Cui, C. Huang, Q. Xiao, In Vitro Interaction Investigation between Three Ru(II) Arene Complexes and Human Serum Albumin: Structural Influences. *RSC Adv.* 6 (2016), 47043–47054. (b) L. Colina-Vegas, L. Luna-Dulcey, A. M. Plutín, E. E. Castellano, M. R. Cominetti, A. A. Batista, Half Sandwich Ru(II)-Acylthiourea Complexes: DNA/HSA-Binding, Anti-Migration and Cell Death in a Human Breast Tumor Cell Line. *Dalton Trans.* 46 (2017), 12865–12875. (c) J. Sun, Y. Huang, C. Zheng, Y. Zhou, Y. Liu, J. Liu, Ruthenium (II) Complexes Interact with Human Serum Albumin and Induce Apoptosis of Tumor Cells. *Biol. Trace Elem. Res.* 163 (2015), 266–274. (d) K. M. Oliveira, R. S. Corrêa, M. I. F. Barbosa, J. Ellena, M. R. Cominetti, A. A. Batista, Ruthenium(II)/Triphenylphosphine Complexes: An Effective Way to Improve the Cytotoxicity of Lapachol, *Polyhedron* 130 (2017), 108–114.
- ³⁵ E. Nissani, B. Perlmutter-Hayman, Drug-Binding to Biological Macromolecules. A Kinetic Study of the System Chlorodiazepoxide (Librium) and Bovine Serum Albumin. *Int. J. Chem. Kinet.* 18 (1986), 1123–1132.
- ³⁶ N. Busto, J. Valladolid, C. Aliende, F. A. Jalón, B. R. Manzano, A. M. Rodríguez, J. F. Gaspar, C. Martins, T. Biver, G. Espino, J. M. Leal, B. García, Preparation of Organometallic Ruthenium–Arene–Diaminotriazine Complexes as Binding Agents to DNA. *Chem. Asian J.* 7 (2012), 788–801.

- 37 R. K. Gupta, A. Kumar, R. P. Paitandi, R. S. Singh, S. Mukhopadhyay, S. P. Verma, P. Das, D. S. Pandey, Heteroleptic Arene Ru(II) Dipyrrinato Complexes: DNA, Protein Binding and Anti-Cancer Activity against the ACHN Cancer Cell Line. *Dalton Trans.* 45 (2016), 7163–7177.
- 38 (a) L. Chen, H. Chao, Q. Zhao, H. Li, Unique Optical Oxygen-Sensing Performance of $[\text{Ru}(\text{IP})_2(\text{HNAIP})]^{2+}$ during the Groove-Binding-Induced B-to-Z DNA Conformational Transition. *Inorg. Chem.* 54 (2015), 8281–8287. (b) M. Ganeshpandian, M. Palaniandavar, A. Muruganantham, S. K. Ghosh, A. Riyasdeen, M. A. Akbarsha, Ruthenium(II)–Arene Complexes of Diimines: Effect of Diimine Intercalation and Hydrophobicity on DNA and Protein Binding and Cytotoxicity. *Appl. Organomet. Chem.* 32 (2018), e4154.
- 39 M. Ganeshpandian, R. Loganathan, E. Suresh, A. Riyasdeen, M. A. Akbarsha, M. Palaniandavar, New Ruthenium(II) Arene Complexes of Anthracenyl-Appended Diazacycloalkanes: Effect of Ligand Intercalation and Hydrophobicity on DNA and Protein Binding and Cleavage and Cytotoxicity. *Dalton Trans.* 43 (2013), 1203–1219.
- 40 J. B. Chaires, A Thermodynamic Signature for Drug–DNA Binding Mode. *Arch. Biochem. Biophys.* 453 (2006), 26–31.
- 41 (a) F. Guarra, N. Busto, A. Guerri, L. Marchetti, T. Marzo, B. García, T. Biver, C. Gabbiani, Cytotoxic Ag(I) and Au(I) NHC-carbenes bind DNA and show TrxR inhibition, *J. Inorg. Biochem.* 2020, 205, 110998. (b) S. K. Tripathy, A. C. Taviti, N. Dehury, A. Sahoo, S. Pal, T. K. Beuria, S. Patra, *Dalton Trans.*, 2015, 44, 5114–5124. (c) A. K. Pradhan, P. Mondal, *Computational Theor. Chem.* 2020, 1172, 112664.
- 42 (a) B. García, J. M. Leal, R. Ruiz, T. Biver, F. Secco, M. Venturini, *J. Phys. Chem. B* 2010, 114, 25, 8555–8564. (b) M. Ganeshpandian, R. Loganathan, E. Suresh, A. Riyasdeen, M. Abdulkadher Akbarshade, M. Palaniandavar, New ruthenium(ii) arene complexes of anthracenyl-appended diazacycloalkanes: effect of ligand intercalation and hydrophobicity on DNA and protein binding and cleavage and cytotoxicity, *Dalton Trans.*, 2014, 43, 1203–1219.
- 43 (a) J. M. Kliegman, R. K. Barnes, Conjugated aliphatic diimines from glyoxal and aliphatic primary amines, *Tetrahedron* 1970 (26) 2555–2560; (b) I. E. Buys, S. Elgafi, L. D. Field, T. W. Hambley, B. A. Messerle, Formation of a Novel Dipyrrrolopyrrole Mediated by a 1,4-Diaza-1,3-diene Complex of Iron, *Inorg. Chem.* 33 (1994) 1539–1542.
- 44 H. E. Gottlieb, V. Kotlyar, A. Nudelman, NMR Chemical Shifts of Common Laboratory Solvents as Trace Impurities, *J. Org. Chem.* 62 (1997) 7512–7515.
- 45 R. K. Harris, E. D. Becker, S. M. Cabral del Menezes, R. Goodfellow, P. Granger, NMR Nomenclature. Nuclear spin properties and conventions for chemical shifts *Pure Appl. Chem.* 73 (2001) 1795–1818.
- 46 F. Menges, "Spectragryph - optical spectroscopy software", Version 1.2.14d, @ 2016–2020, <http://www.effemm2.de/spectragryph>.

- 47 W. J. Geary, The use of conductivity measurements in organic solvents for the characterization of coordination compounds, *Coord. Chem. Rev.* 7 (1971) 81-122.
- 48 Sheldrick, G. M. *SADABS-2008/1 - Bruker AXS Area Detector Scaling and Absorption Correction*, Bruker AXS: Madison, Wisconsin, USA, 2008.
- 49 G. M. Sheldrick, Crystal structure refinement with SHELXL ActaCryst. C 71 (2015), 3-8.
- 50 T. Rundlöf, M. Mathiasson, S. Bekiroglu, B. Hakkarainen, T. Bowden, T. Arvidsson, Survey and qualification of internal standards for quantification by ¹H NMR Spectroscopy. *J. Pharm. Biomed. Anal.* 52 (2010) 645–651.
- 51 N. M. Rice, H. M. N. H. Irving, M. A. Leonard, Nomenclature for liquid-liquid distribution (solvent extraction). *Pure Appl. Chem.* 65 (1993) 2373-2396.
- 52 (a) OECD Guidelines for Testing of Chemicals. In OECD, Paris: 1995; Vol. 107. (b) J. C. Dearden,; G. M. Bresnen, The Measurement of Partition Coefficients, *Quant. Struct.-Act. Relat.* 7 (1988) 133-144. (c) Optimized procedure: G. Agonigi, L. Biancalana, M. G. Lupo, M. Montopoli, N. Ferri, S. Zacchini, F. Binacchi, T. Biver, B. Campanella, G. Pampaloni, V. Zanotti, F. Marchetti, Exploring the Anticancer Potential of DiironBis-cyclopentadienyl Complexes with Bridging Hydrocarbyl Ligands: Behavior in Aqueous Media and In Vitro Cytotoxicity. *Organometallics* 39 (2020) 645-657.
- 53 Calculated by the formula $pD = pH^* + 0.4$, where pH^* is the value measured for H₂O-calibrated pH-meter. (a) C. C. Westcott, pH Measurements; Academic Press: New York, 1978. (b) A. K. Covington, M. Paabo, R. A. Robinson, R. G. Bates. Use of the glass electrode in deuterium oxide and the relation between the standardized pD (paD) scale and the operational pH in heavy water. *Anal. Chem.* 40 (1968), 700-706.
- 54 H. M. E. Azzazy, R. H. Christenson, All About Albumin: Biochemistry, Genetics, and Medical Applications. *Clin. Chem.* 43 (1997), 2014–2016].
- 55 G. Felsenfeld, S. Z. Hirschman, A Neighbor-Interaction Analysis of the Hypochromism and Spectra of DNA. *J. Mol. Biol.* 13 (1965), 407–427.
- 56 M. J. Waring, Complex Formation between Ethidium Bromide and Nucleic Acids. *J. Mol. Biol.* 13 (1965), 269–282.
- 57 Clinical and Laboratory Standards Institute. 2012. Performance standards for antimicrobial susceptibility testing: 17th informational supplement M07-A9. Clinical and Laboratory Standards Institute, Wayne, P.